

AD-A081 900

AIR FORCE INST OF TECH WRIGHT-PATTERSON AFB OH SCHOO--ETC F/8 1/3
EFFECTS OF GEOMETRIC VARIABLES ON STRESS INTENSITY FACTORS FOR --ETC(U)
DEC 78 M CARMON
AFIT/6AE/AA/78D-3

UNCLASSIFIED

Nil

$$\frac{1}{\Delta t} \int_{\Delta t}^{\Delta t + \Delta t} \frac{d}{dt} \left(\frac{1}{2} \rho \mathbf{u} \cdot \mathbf{u} \right) dt$$

■

END
DATE
FILMED
4-80
DTIC

AFIT/GAE/AA/78D-3

EFFECTS OF GEOMETRIC VARIABLES
ON STRESS INTENSITY FACTORS FOR
CRACK GAGES

THESIS

AFIT/GAE/AA/78D-3 ✓

Benjamin Cannon
Major IAF

Approved for public release; distribution unlimited.

DTIC
SELECTED
MAR 18 1980
A

14
AFIT/GAE/AA/78D-3

6
EFFECTS OF GEOMETRIC VARIABLES
ON STRESS INTENSITY FACTORS FOR
CRACK GAGES

9
Mavston's THESIS

12, 1978

Presented to the Faculty of the School of Engineering
of the Air Force Institute of Technology
Air University
in Partial Fulfillment of the
Requirements for the Degree of
Master of Science

10) by
Menachem Carmon

Major IAF

Graduate Aeronautical Engineering

11) December 1978

Approved for public release; distribution unlimited

014415

Preface

At this opportunity I would like to express my gratitude to my thesis advisor, Dr. P. J. Torvik for his inspiring guidance and fruitful suggestions during the course of the study. Also special thanks are due to Dr. V. B. Venkayya and Mrs. V. A. Tischler from AFFDL/FBR for their devotion and aid in obtaining the finite element analysis used in this study. I would also like to thank Dr. A. F. Grandt from AFML for his aid and advice, and Mr. T. D. Gray and Captain D. Holloway from AFFDL/FBE who sponsored this study. I would also like to thank the staff of the Fracture Laboratory of AFFDL, Mr. H Stalnaker, Mr. R. Kleinsmit, Mr. Jack Smith, and Mr. Larry Bates for performing some of the tests required. Finally, I deeply thank my wife Ella for sharing with me the experience of this study and for her contribution to the completion of this work.

Contents

	Page
Preface	ii
List of Figures	v
List of Tables	vii
Notations	viii
Abstract	x
I. Introduction	1
Background	1
Crack Gage Concept	2
Statement and Scope of Problem	4
II. Stress Intensity Factor Solution for a Cracked Flat Sheet subjected to Mixed Boundary Condition	6
Introduction	6
Method of Solution	6
III. Stress Intensity Factor Solution for a Trapezoidal, Edge Cracked Crack Gage with Prescribed End Displacement	15
Results and Discussion	17
IV. Stress Intensity Factor Solution for a Stepped Center Crack - Crack Gage, with Prescribed End Displacements.	20
Methods of Solution	20
Numerical Evaluation.	26
Results and Discussion	27
V. Experimental Results	43
VI. Conclusions and Recommendations	48
Conclusions	48
Recommendations	48
.	
Bibliography	50
Appendix A: Stress and Displacements as Result of Williams' Stress Function	52

	Page
Appendix B: Description of Computer Programs	55
Appendix C: Finite Element Solution	57
Appendix D: Stepped Center Gage-Stress Intensity Factor Approximation Equation	60
Vita	62

List of Figures

Figure		Page
1	Crack Gage Concept	3
2	Mixed Boundary Condition Problem	7
3	Trapezoid Crack Gage	16
4	Stress Intensity Factor for Trapezoid Crack Gage $H_c/b = 1$	18
5	Stress Intensity Factor for Trapezoid, Crack Gage $H_a/b = 1$	19
6	Center Crack, Stepped Gage Geometry	21
7	Center Portion of the Stepped Gage with Boundary Conditions	22
8	Stepped Crack Gage - Outer Segment	23
9	Comparison of Stress Intensity Values for Center Cracked Uniform Thickness Gage and Stepped Gage .	32
10	Stress Intensity Factor Results for Gage with $t_c/t_o = .2$ $L_c/b = .2$	33
11	Stress Intensity Factor Results for Gage with $t_c/t_o = .2$, Various Length Ratios	34
12	Stress Intensity Factor Results for Gage with $t_c/t_o = .2$ $L_c/b = .625$	35
13	Stress Intensity Factor Results for Gages with $t_c/t_o = .5$ $L_c/b = .2$	36
14	Stress Intensity Factor Results for Gages with $t_c/t_o = .5$, Various Length Ratios	37
15	Stress Intensity Factor Results for Gages with $t_c/t_o = .5$, $L_c/b = .625$	38
16	Stress Intensity Factor Results for Gages with $t_c/t_o = .75$, $L_c/b = .2$	39
17	Stress Intensity Factor Results for Gages with $t_c/t_o = .75$, Various Length Ratios	40

Figure		Page
18	Stress Intensity Factor Results for Gages with $t_c/t_o=.75$, $L_c/b=.625$	41
19	Stress Intensity Factor Results for $L_c/L_o=.315$, $L_c/L_o=.312$	42
20	Tested Stepped Gage Schematic Geometry	45
21	Carrying Specimen with Typical Crack Gage Arrange- ment	46
22	Comparison Between Caclulated Stress Intensity Factor and Experimental Results. Gage Dimensions $t_c/t_o=.2$, $L_c/L_o =1.0$	47
23	Finite Element Model and Mesh Organization for Outer Segment of Gage	58
24	Displacement of Membrane Edge due to Uniform Stress	59
25	Schematic Stress Distribution at Crack Tip	61

List of Tables

Table		Page
I	Convergence of Stress Intensity Factor $K_I/\sigma_S\sqrt{b}$. . .	29
II	Convergence of Stress Int nsity Factor $K_I/\sigma_S\sqrt{b}$. . .	29
III	Stress Intensity Factor for Stress Loading - Compari- son with Published Results	30

Notations

a	Crack length
A_n	Williams' stress function expansion coefficients
A_{mq}	Matrix element
$b, 2b$	Gage width for edge cracked gage and center cracked gage, respectively
c	Constant
d_m	Expansion coefficient
E	Young modulus
e	Strain
F_q	"loading vector"
F_i	Body forces
H_c	Half length of the cracked edge in a trapezoid gage
H_a	Half length of the uncracked edge opposite to crack edge in a trapezoid gage
J	Reissner's functional
K_I	Stress Intensity Factor
L	Length of stepped gage
L_T	Half total length of a stepped gage
M	Half number of terms in stress and displacement expansion
N	Number of cycles
n	Number of nodal points on edge
P	Force
r	Radial coordinate in polar system
S	Surface
$[S]$	Flexibility Matrix
T	Traction

t	Thickness
U	Displacement
V	Volume
W	Strain energy density
x	Coordinate
y	Coordinate

Subscripts

c	Center segment
g	Gage
i,j, k,l, m,n, q	Indices
O	Outer segment
r	Radial direction
s	Structure
T	Traction only prescribed
Tu	Traction and displacement prescribed
u	Displacement only prescribed

Superscript

k,m, o,p	Indices
*	Prescribed

Abstract

A cracked metallic coupon, called crack gage, is being considered as a device for monitoring crack growth in aircraft structures. For this purpose, a stress intensity factor solution for the gage has to be known.

This study provides stress intensity factor solutions for two basic geometric configurations subjected to prescribed displacements.

1. Edge cracked, trapezoidal shaped gages of uniform thickness.
2. Center cracked gages with varying or stepped thickness.

For the trapezoid, the influences of changing the length of the cracked edge, while other edge remains constant, and vice versa, were investigated. The results obtained do not show significant beneficial changes in stress intensity factor for the range of parameters considered over those of rectangular gages.

Stress intensity factors were determined for stepped gages of various geometries. Various thickness ratios, length ratios and aspect ratios were considered, including the specific geometries of two gages now under development. In each case, the stress intensity factor was determined as a function of crack length.

Stress intensity factors were found to increase as the cracked center portion was made thinner, and as the length of the outer section was increased. The stepped gage was found to have the potential for tailoring the stress intensity factor. Finally, analytical results of stress intensity factor were found to show good agreement with experimental results.

EFFECT OF GEOMETRIC VARIABLES ON STRESS

INTENSITY FACTORS FOR CRACK GAGES

I. Introduction

Background

The concept and the requirements for safety, durability and management of military aircraft structures are summarized by Coffin and Tiffany (Ref 1). As reflected there, the durability analysis as well as scheduled maintenance for the structure are based on some assumed usage of the fleet. Usually the actual usage of an individual aircraft and the fleet will differ from the usage for which the aircraft was designed. In order to provide updated usage data for force management, MIL STD 1530A(11) (Ref 2:23-25) requires establishing aircraft structures tracking programs. Such a program provides baseline operational load spectra for average fleet usage as well as an Individual Airplane Tracking (IAT) program, which provides crack growth information concerning each individual aircraft. The IAT is the feedback link necessary for the scheduling of structural maintenance.

A typical, current technology, IAT program is that of the F-4 aircraft. This program was developed as part of the Damage Tolerance Assessment Study for F/RF-4 C/D and F-4E(S) aircraft (Ref 3, 4). The program uses as tracking devices counting accelerometers installed on each aircraft and flight data recorders installed on 12% of the fleet. A crack growth analysis is performed for critical structural locations. Stress exceedances spectra for each critical location and for different

usage categories were developed from the flight recorded data. These spectra along with counting accelerometer exceedances readings are used to determine the stress history at critical locations. Using these, a crack growth analysis for an individual aircraft may be performed.

This tracking system, described in more detail in other places (Ref 3, 4, 5, 6:64-66), is very indirect in defining stresses and involves many sources for error. Further, the enormous amount of data to be collected in order to get the stresses adds to program cost. A device, the crack gage, has been proposed which might provide a more direct and efficient technique for use in IAT programs. It has been estimated that using crack gages in the F-4 IAT program might save 7.7 million dollars in five years (Ref 6:79).

Crack Gage Concept

A preliminary concept of a crack gage was patented by Smith (Ref 7) in 1976. A more practical concept for using a crack gage for monitoring structure crack was introduced by Crane, Gallagher and Grant (Ref 8). Figure 1 shows the concept of the crack gage. It consists of a pre-cracked thin metallic sheet with ends bonded to a structure. Since the structure and the gage will be exposed to the same load history, it is possible to relate the crack growth in the structure to that in the gage. The readily observed crack growth in the gage can then be used as a prediction of crack growth in the structure.

Efforts in various directions were made in evaluating the crack gage concept since it has been introduced. Torvik (Ref 9, 10) developed an analytical solution for the stress intensity factor for displacement

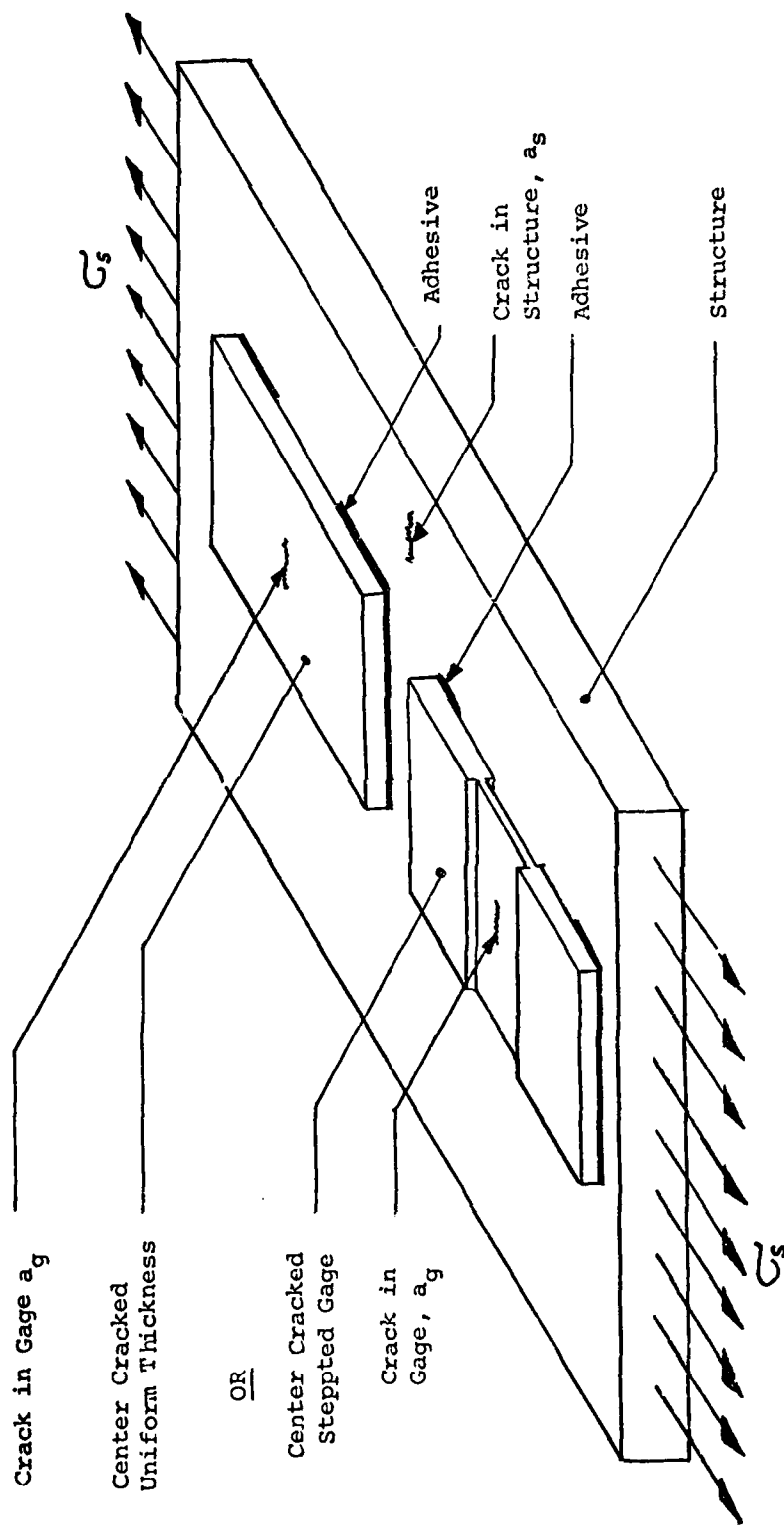


Figure 1. Crack Gage Concept

controlled, edge cracked gages. Ori (Ref 11) and Ashbaugh and Grandt (Ref 12) evaluated the concept using both edge cracked and center cracked gages.

Stepped center cracked gages are now being investigated under two U.S. Air Force contracts, one with Boeing Wichita (Ref 13) and one with McDonnell Douglas Corporation (Ref 14). The contract with McDonnell Douglas will provide evaluation of a center cracked stepped gage on a F-4 aircraft during a full scale fatigue test.

Statement and Scope of Problem

It has been observed (Ref 9, 10) that relatively high stress intensity factors for an edge cracked rectangular gage may be obtained if the gage is long, but the magnitude then varies considerably as the crack grows. On the other hand, constant stress intensity factor vs crack length may be obtained for relatively short gages, but the gage sensitivity is then very low. For analytical purposes, such as predicting the remaining life of a structure, a constant stress intensity factor vs crack length is desired. It was suggested that an edge-cracked gage of a trapezoidal planform might satisfy the requirement for a higher, but constant K_I vs. crack length, since the "effective" length of the gage could vary as the crack grows. The stepped gage was also considered since the thicker section serves as an amplifier of the strain in the cracked section from the far field value. The gain may be controlled by varying the thickness ratios and length ratios of the segments of the gage.

The gages that had been developed for the activities previously mentioned were basically developed empirically. It became apparent

that an analytical method that could be used to obtain stress intensity factor solution for stepped center cracked gages was required. Gages with different stress intensity factor sensitivities are required so that the gage can be matched to the specific usage, i.e., applying gages of very high sensitivity to structures to be subjected to a large number of cycles.

In this study, a means of obtaining analytical predictions of the stress intensity factor for the two geometries, trapezoidal planform and stepped gages, is developed. These methods are applied to the design of crack gage and the results for the stepped gage were experimentally verified.

II. Stress Intensity Factor Solution for a Cracked Flat Sheet Subjected to Mixed Boundary Conditions

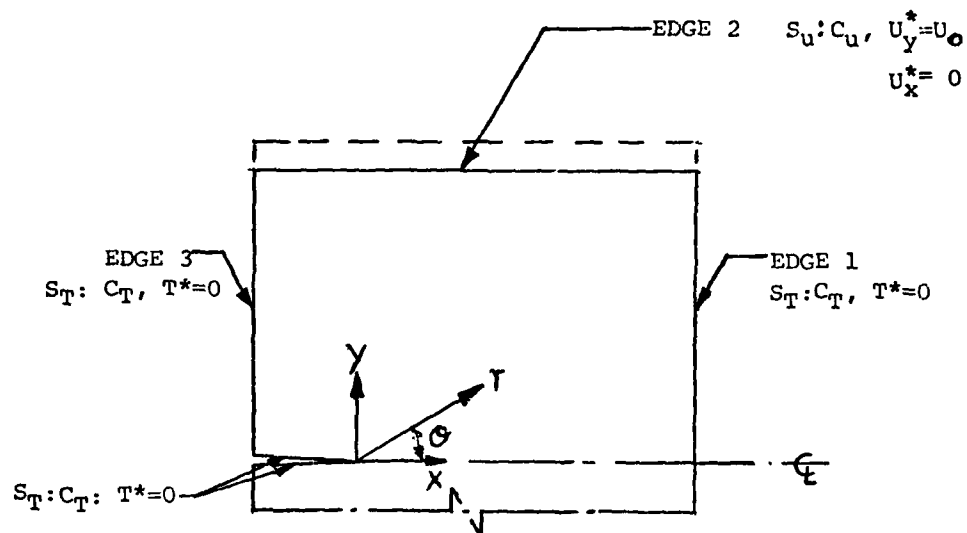
Introduction

A method utilizing Williams' (Ref 15, 16) stress functions along with energy principles was developed by Torvik (Ref 9, 10) to obtain a stress intensity factor solution for a finite, cracked elastic sheet. Solutions were provided for a rectangular edge cracked sheet subjected to mixed boundary conditions. Part of the boundary was subjected to prescribed tractions as shown in Figure 2A, herein referred to as the type 1-mixed boundary condition. The solution for a center cracked sheet, which is the center section of the stepped cracked gage, led to a different mixed boundary condition, herein referred to as type 2, and shown in Figure 2B. For this problem, a part of the region of the physical surface is subjected simultaneously to prescribed tractions as well as to displacements. A brief outline of the method developed by Torvik (Ref 9, 10), for the type 1-mixed boundary condition problem, and the necessary extension for the type 2-boundary condition problem, will be presented here.

Method of Solution

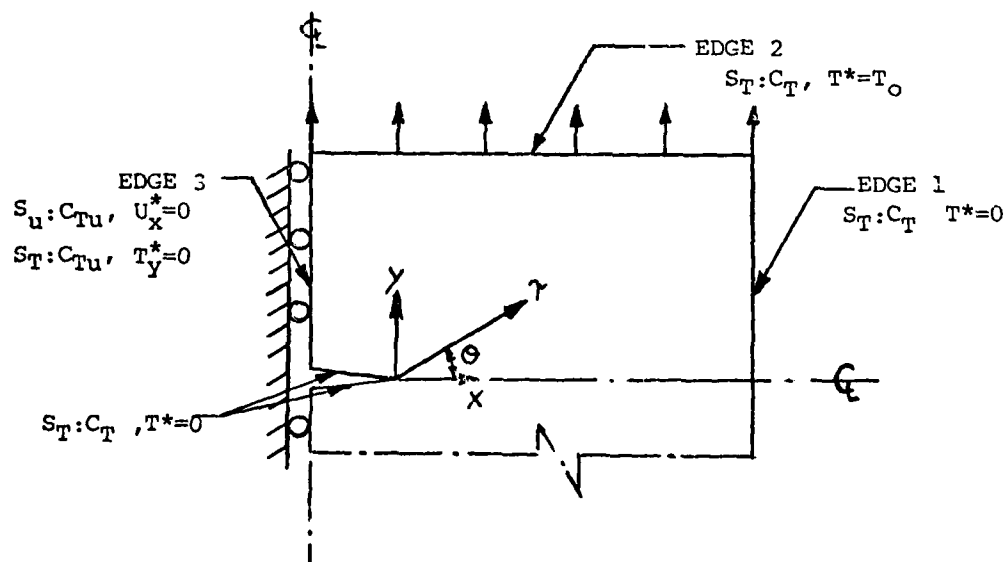
Consider a thin elastic sheet for which plane stress conditions hold, with a crack, starting at an edge. A coordinate system is set with origin placed at crack tip. The crack faces are located at $\theta = \pm\pi$, $0 \leq r \leq a$, and are free of tractions. Williams (Ref 15, 16) has shown that for an infinite domain, stress fields can be obtained by using a stress function of the form

$$\chi(r, \theta, \lambda) = r^{\lambda+1} F(\theta, \lambda) \quad (1)$$



(a) Type 1, Mixed Boundary Conditions

- No mix between prescribed traction and displacement on same region



(b) Type 2, Mixed Boundary Conditions

- Prescribed stresses and displacements on same region

Figure 2. Mixed Boundary Conditions Problem.

$$\lambda = m/2 \quad \text{for } m = 1, 2, 3, \dots \quad (2)$$

The stress function may be divided into even and odd parts. Since the geometries of interest for this study are symmetric in respect to X axis, only the even part of the stress function is of interest. In addition, displacements corresponding to the stress function may be found from

$$2\mu U_r = -\frac{\partial \chi}{\partial r} + (1-s)r\frac{\partial \psi}{\partial \theta} \quad (3)$$

$$2\mu U_\theta = -\frac{1}{r}\frac{\partial \chi}{\partial \theta} + (1-s)r^2\frac{\partial \psi}{\partial r} \quad (4)$$

$$\mu = \text{shear modulus} \quad s = \nu/1+\nu \quad \nu = \text{Poisson ratio}$$

$$\nabla^2 \chi = \frac{\partial}{\partial r}\left(r\frac{\partial \psi}{\partial \theta}\right) \quad (5)$$

The even parts of χ and ψ , as well as the corresponding stresses and displacements, are shown in Appendix A. Each stress and displacement is made up from an even and an odd part. As stated by Torvik (Ref 9:3-4, 10), the stresses σ and the displacements U may be represented in the form:

$$\begin{bmatrix} \sigma_{rr} \\ \sigma_{\theta\theta} \\ \sigma_{r\theta} \end{bmatrix} = \sum_{m=1}^M d_m \cdot \begin{bmatrix} \sigma_{rr}^m \\ \sigma_{\theta\theta}^m \\ \sigma_{r\theta}^m \end{bmatrix} \quad (6)$$

where each σ^m satisfies field equations and the traction free requirement on the crack face, and

$$\begin{bmatrix} 2\mu U_r \\ 2\mu U_\theta \end{bmatrix} = \sum_{m=1}^M d_m \cdot \begin{bmatrix} U_r^m \\ U_\theta^m \end{bmatrix} \quad (7)$$

Each of U^m satisfies strain displacement equations and stress strain laws, and the arbitrary coefficients d_m are related to the stress and displacement functions coefficients presented in Appendix A as A_m through the relation

$$d_1 = A_1, d_2 = -A_2, d_3 = -A_3, d_4 = A_4, d_5 = A_5, d_6 = -A_6, \text{ etc.}$$

In order to find a stress intensity factor, defined as,

$$K_I = \lim_{r \rightarrow 0} \{\sqrt{2\pi r} \sigma_{\theta\theta}(\theta = 0, r)\} \quad (8)$$

it will be required to find the stress $\sigma_{\theta\theta}$ for a certain boundary condition problem. More specifically, the coefficients d_m in Eq (6) are to be obtained.

After applying the limit procedure, the only term to remain is the one multiplied by d_1 . All other terms vanish since they include r^p expressions, $p \geq 1/2$. Hence,

$$K_I = \sqrt{2\pi} A_1 = -\sqrt{2\pi} d_1 \quad (9)$$

The solution of the coefficients for a mixed boundary condition of type 1 was given by Torvik (Ref 9:20-21, 10) utilizing Reissner's principle. The interpretation of Reissner's principle by Fung (Ref 17:299-300) is that the surface S enclosing the domain V , can be divided into S_T and S_u , where tractions are prescribed on S_T and displacements on S_u . A more general interpretation will be presented here.

In the type 2 mixed boundary condition, a surface region C_{Tu} on the surface S can be subjected simultaneously to prescribed tractions and displacements as well. Hence, it may be considered a subset of S_T as well as S_u , with the relations:

$$S = S_T + S_u \quad (10)$$

$$S_T = C_T + C_{Tu} \quad (11)$$

$$S_u = C_u + C_{Tu} \quad (12)$$

where C_T is the region where only tractions are prescribed, and C_u is the region where only displacements are prescribed.

Consider the functional (essentially Reissner's function)

$$J = \int_V [W(e_{ij}) - F_i U_i] dv - \int_V \sigma_{ij} [e_{ij} - 1/2(U_{i,j} + U_{j,i})] dv - \\ - \int_{S_T} T_i^* U_i ds - \int_{S_u} \sigma_{ij} v_j (U_i - U_i^*) ds \quad (13)$$

Where stresses, displacements and strains are to be independent variables, and $\sigma_{ij} = \sigma_{ji}$. The elastic equilibrium will be obtained by setting $J = 0$, or J will be stationary with $J = 0$. The Q_{ij} are introduced as Lagrange multipliers.

$$\delta J = 0 = \int_V \left(\frac{\partial W}{\partial e_{ij}} \delta e_{ij} - F_i \delta U_i \right) dv - \int_V \delta \sigma_{ij} [e_{ij} - 1/2(U_{i,j} + U_{j,i})] dv - \\ - \int_V \sigma_{ij} [\delta e_{ij} - 1/2(\delta U_{i,j} + \delta U_{j,i})] dv - \int_{S_T} T_i^* \delta U_i ds - \\ - \int_{S_u} \delta (v_j \sigma_{ij}) \cdot (U_i - U_i^*) ds - \int_{S_u} v_j \sigma_{ij} \delta U_i ds \quad (14)$$

Rearranging and applying the divergence theorem to third integral, we find

$$\delta J = 0 = \int_V \left(\frac{\partial W}{\partial e_{ij}} - \sigma_{ij} \right) \delta e_{ij} dv - \int_V \left(F_i + \frac{\partial \sigma_{ij}}{\partial x_j} \right) \delta U_i dv - \int_V \delta \sigma_{ij} [e_{ij} - \\ - 1/2(U_{i,j} + U_{j,i})] dv + \int_S v_j \sigma_{ij} \delta U_i ds - \int_{S_T} T_i^* \delta U_i ds - \\ - \int_{S_u} (U_i - U_i^*) \delta T_i ds - \int_{S_u} T_i \delta U_i ds \quad (15)$$

Realizing that the first three integrals represent the stress-strain law, equation of equilibrium and strain displacement equation respectively, they may be omitted from Eq (15) if we choose the stresses to be represented by Eq (6), and displacements by Eq (7), along with the corresponding strain.

Eq (15) reduces to:

$$\int_S v_j \sigma_{ij} \delta u_i ds - \int_{S_T} T_i^* \delta u_i ds - \int_{S_u} (u_i - u_i^*) \delta T_i ds - \int_{S_u} T_i \delta u_i ds = 0 \quad (16)$$

$$\int_{S_T} (T_i - T_i^*) \delta u_i ds - \int_{S_u} (u_i - u_i^*) \delta T_i ds = 0 \quad (17)$$

Applying Eqs (11) and (12)

$$\begin{aligned} & \int_{C_T} (T_i - T_i^*) \delta u_i ds - \int_{C_u} (u_i - u_i^*) \delta T_i ds + \\ & + \int_{C_{Tu}} \left[(T_{(i)} - T_{(i)}^*) \delta u_{(i)} - (u_{(j)} - u_{(j)}^*) \delta T_{(j)} \right] ds = 0 \quad (18) \end{aligned}$$

where $j \neq i$, and the parentheses indicate suspension of the summation convention. On C_{Tu} , one component each of displacement and traction are given.

Eq (18) may be used to find a K_I solution for problems with mixed boundary condition of type 2.

Use now the stresses and displacements as defined in Eq (6) and (7) to find variations of stress and displacement.

$$\delta \sigma_{ij} = \sum_{p=1}^M \delta d_p \sigma_{ij}^p \quad (19)$$

$$2\mu \begin{bmatrix} \delta U_r \\ \delta U_\theta \end{bmatrix} = \sum_{p=1}^M \delta d_p \begin{bmatrix} U_r^p \\ U_\theta^p \end{bmatrix} \quad (20)$$

Substituting Eqs (6), (7), (19) and (20) into Eq (18):

$$\begin{aligned} & \int_{C_T} [(v_j \sum_{m=1}^M d_m \sigma_{ij}^m - T_i^*) \frac{1}{2\mu} \sum_{p=1}^M \delta d_p U_i^p] ds - \\ & - \int_{C_u} [(\sum_{m=1}^M d_m U_i^m - 2\mu U_i^*) v_j \sum_{p=1}^M \delta d_p \sigma_{ij}^p] ds - \\ & + - \int_{C_{Tu}} [(v_j \sum_{m=1}^M d_m \sigma_{(i)j}^m - T_{(i)}^*) \frac{1}{2\mu} \sum_{p=1}^M \delta d_p U_{(i)}^p - \\ & - \frac{1}{2\mu} (\sum_{m=1}^M d_m U_{(j)}^m - 2\mu U_{(j)}^*) v_i \sum_{p=1}^M \delta d_p \sigma_{i(j)}^p] ds = 0 \end{aligned} \quad (21)$$

Since δd_p is arbitrary, make the choice $\delta d_p = 0$, $p \neq q$, $\delta d_p = 1$ if $p=q$ and then:

$$\begin{aligned} & \int_{C_T + C_{Tu}} (v_j \sum_{m=1}^M d_m \sigma_{ij}^m) U_i^q ds - \int_{C_u + C_{Tu}} (\sum_{m=1}^M d_m U_i^m) v_j \sigma_{ij}^q ds = \\ & = \int_{C_T} T_i^* \cdot U_i^q ds - \int_{C_{Tu}} [T_i^* \cdot U_i^q ds - 2\mu U_i^* \cdot T_i^q] ds - 2\mu \int_{C_u} U_i^* \cdot T_i^q ds \end{aligned} \quad (22)$$

Eq (22) may be represented as:

$$\sum_{m=1}^M d_m A_{mq} = F_q \quad (23)$$

where A_{mq} is a symmetric matrix.

$$\begin{aligned}
A_{mq} = & \int_{C_T + C_{Tu}} [(\nu_r \sigma_{rr}^m + \nu_\theta \sigma_{r\theta}^m) U_r^q + (\nu_r \sigma_{\theta r}^m + \nu_\theta \sigma_{\theta\theta}^m) U_\theta^q] ds - \\
& - \int_{C_u + C_{Tu}} [U_\theta^m (\nu_r \sigma_{r\theta}^q + \nu_\theta \sigma_{\theta\theta}^q) + U_r^m (\nu_r \sigma_{rr}^q + \nu_\theta \sigma_{r\theta}^q)] ds
\end{aligned} \quad (24)$$

The reader is reminded that only one product of force and displacement is to be evaluated in the contribution of C_{Tu} to each of these integrals.

$$\begin{aligned}
F_q = & \int_{C_T} (T_r^* U_r^q + T_\theta^* U_\theta^q) ds - 2\mu \int_{C_u} (U_\theta^* T_\theta^q + U_r^* T_r^q) ds - \\
& - \int_{C_{Tu}} [T_r^* U_r^q + T_\theta^* U_\theta^q - 2\mu (U_\theta^* T_\theta^q + U_r^* T_r^q)] ds
\end{aligned} \quad (25)$$

Since the displacements are prescribed elsewhere, the crack tip has to be allowed to translate. Thus, as stated (Ref 9:20, 10), we may introduce a translation term into the expansion, which will be

$$2\mu U_r = d_0 U_i^0 = d_0 \cos \theta \quad (26)$$

$$2\mu U_\theta = d_0 U_i^0 = -d_0 \sin \theta \quad (27)$$

with σ_{rr}^0 , $\sigma_{\theta\theta}^0$, $\sigma_{r\theta}^0$ being zero.

By solving Eq (23) along with Eqs (24) and (25) for the coefficients, d_m a solution for a finite, two dimensional, cracked elastic sheet with mixed boundary conditions of type 2 is obtained. Note, that by eliminating the integral on C_{Tu} region, we get a type 1 mixed boundary problem, and A_{mq} and F_q will have the same form as shown (Ref 9:23, 10) previously.

Since the particular gage geometries for this study are the trapezoidal gage and the stepped gage, the formulation for getting A_{mq} and F_q for these geometries will be shown.

The basic boundary conditions for the trapezoidal gage are essentially as shown in Figure 2a, and the formulation was presented (Ref 9: 23, 10).

$$F_q = 2\mu \int [(U_x \cos \theta + U_y \sin \theta) (v_r \sigma_{rr}^q + v_\theta \sigma_{\theta r}^q) + (-U_x \sin \theta + U_y \cos \theta) \cdot (v_r \sigma_{r\theta}^q + v_\theta \sigma_{\theta\theta}^q)] ds \quad (28)$$

When evaluating A_{mq} for the discussed geometry, crack faces are free of traction. The first integral of Eq (24) will be evaluated on edged 1 and 3, while second integral will be evaluated on edge 2.

The case with boundary conditions shown in Figure 2b represents the center portion of the stepped gage. Edges 1 and 2 are part of C_T , where tractions are prescribed, while edge 3 is part of C_{Tu} .

Taking into account boundary conditions, only a part of the integral C_{Tu} exists on edge 3. Due to boundary condition presentation, A_{mq} and F_q will be represented in cartesian coordinates, and Eq (24) becomes

$$A_{mq} = \int_{C_T} [T_x^m U_x^q + T_y^m U_y^q] ds + \int_{C_{Tu}} [T_y^m U_y^q - U_x^m T_x^q] ds \quad (29)$$

With $C_u = 0$, and with the prescribed variables on C_{Tu} substituted into Eq (25), we get

$$F_q = \int_{C_T} (T_x^m U_x^q + T_y^m U_y^q) ds \quad (30)$$

Those last two equations will be used to solve the stepped crack gage stress intensity problem.

III. Stress Intensity Factor Solution for A Trapezoidal, Edge Cracked Crack Gage with Prescribed End Displacements

The edge cracked rectangular gage has a tendency to give low stress intensity factor values for short gages, while the sensitivity improves for relatively long gages (Ref 9:34-46; 10). This has also been observed in experiments (Ref 6:73). The disadvantage of long gages is that K_I does not remain constant and even decreases as crack grows. This property is not desired for a crack gage. It was thought that giving the gage a trapezoidal shape as shown in Figure 3, a better control on the K_I variation with crack growth, and a higher K_I , might be achieved.

The suggested configuration consists of a thin gage bonded to a structure along the line AB. The structure is loaded by stress σ_s and displacements are transferred to the gage through line AB. The stress intensity factor solution for this case was obtained by using the method shown in Section II. Using Eq (28) along with Eq (24), Eq (23) gives a solution for the coefficient d_1 .

The prescribed displacements are

$$U_y^* = \frac{\sigma_s}{E_s} y \quad (31)$$

$$U_x^* = -xv \frac{\sigma_s}{E_s} \quad (32)$$

$$\text{where } y = Ha - \tan \alpha \cdot (b - x) \text{ and } v = .3 \quad (33)$$

The matrix A_{mq} was evaluated by a computer program (see Appendix B) using an expansion of thirty-six coefficients, including these for rigid body displacements. The integration was performed over 300 boundary points. The variables for this study were chosen to be the

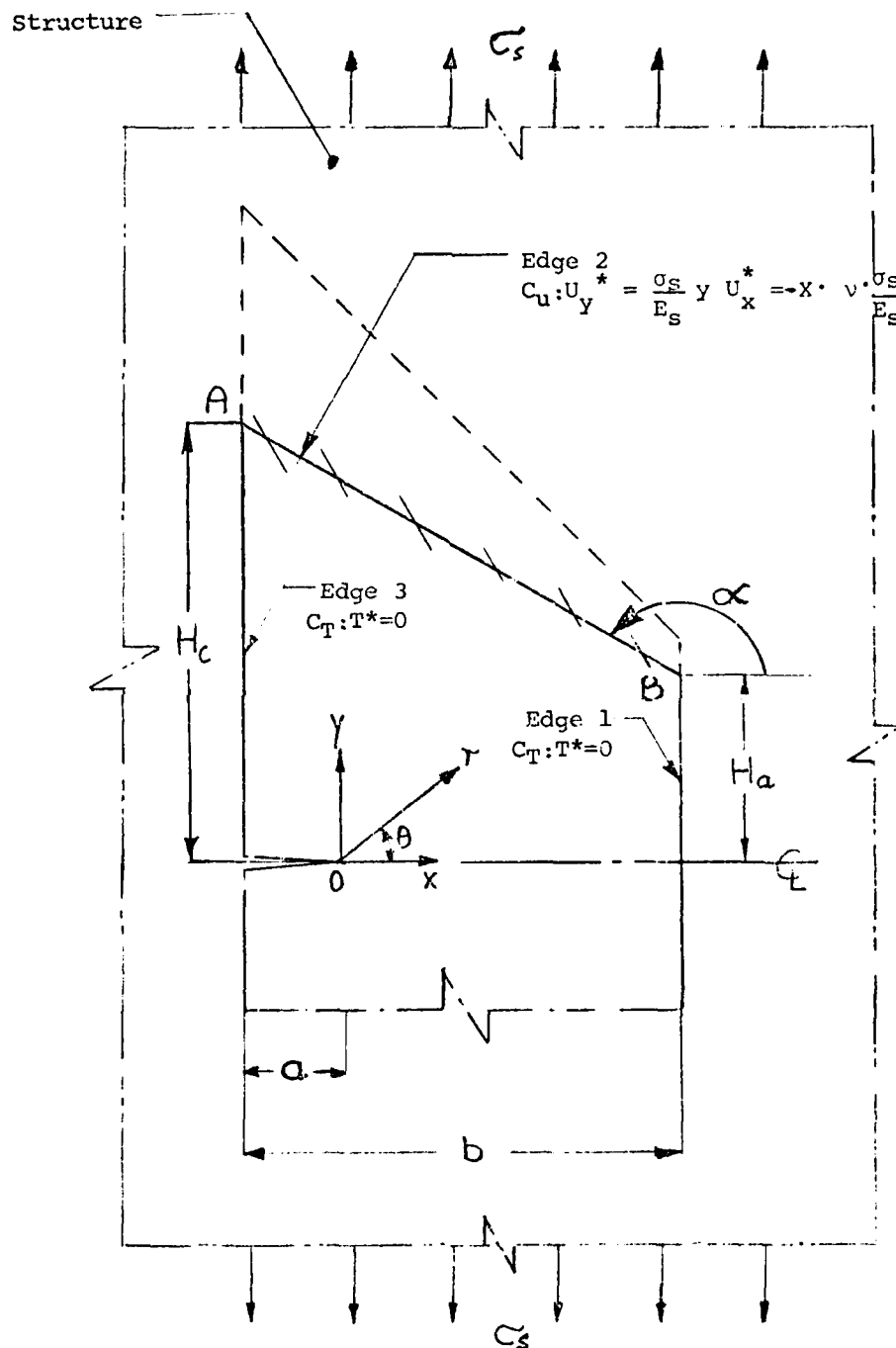


Figure 3. Trapezoid Crack Gage

angle α , which was assumed to control K_I changes as the crack grows, and also to control the magnitude of K_I , since the gage length dimensions are changing. Former results for a rectangular gage (Ref 9:34, 10) indicated that a gage with an aspect ratio of $2 H_a/b=2$ might be a good one for the study, since K_I for that gage was fairly constant as crack length, a , increased.

Results and Discussion

Non-dimensional stress intensity factor results for $H_c/b=1$ are presented in Figure 4. It can be observed that changes in α in the range of $160^\circ - 200^\circ$ have a very little influence on the magnitude of K_I . The general behavior of K_I vs. a improves a little and for $\alpha = 200^\circ$, $K_I/\sigma_s \sqrt{b}$ is almost constant on the range $.4 < a/b < .8$.

Results for $H_a/b \approx 1$ are presented in Figure 5. It can be observed that in comparison to former results the changes in K_I are relatively large as α changes from 165° to 195° . This can be related to the fact that under the displacement loading, the K_I will be more sensitive to length changes on H_c than on H_a since the former directly affects the crack opening, and K_I may be considered proportional to crack opening.

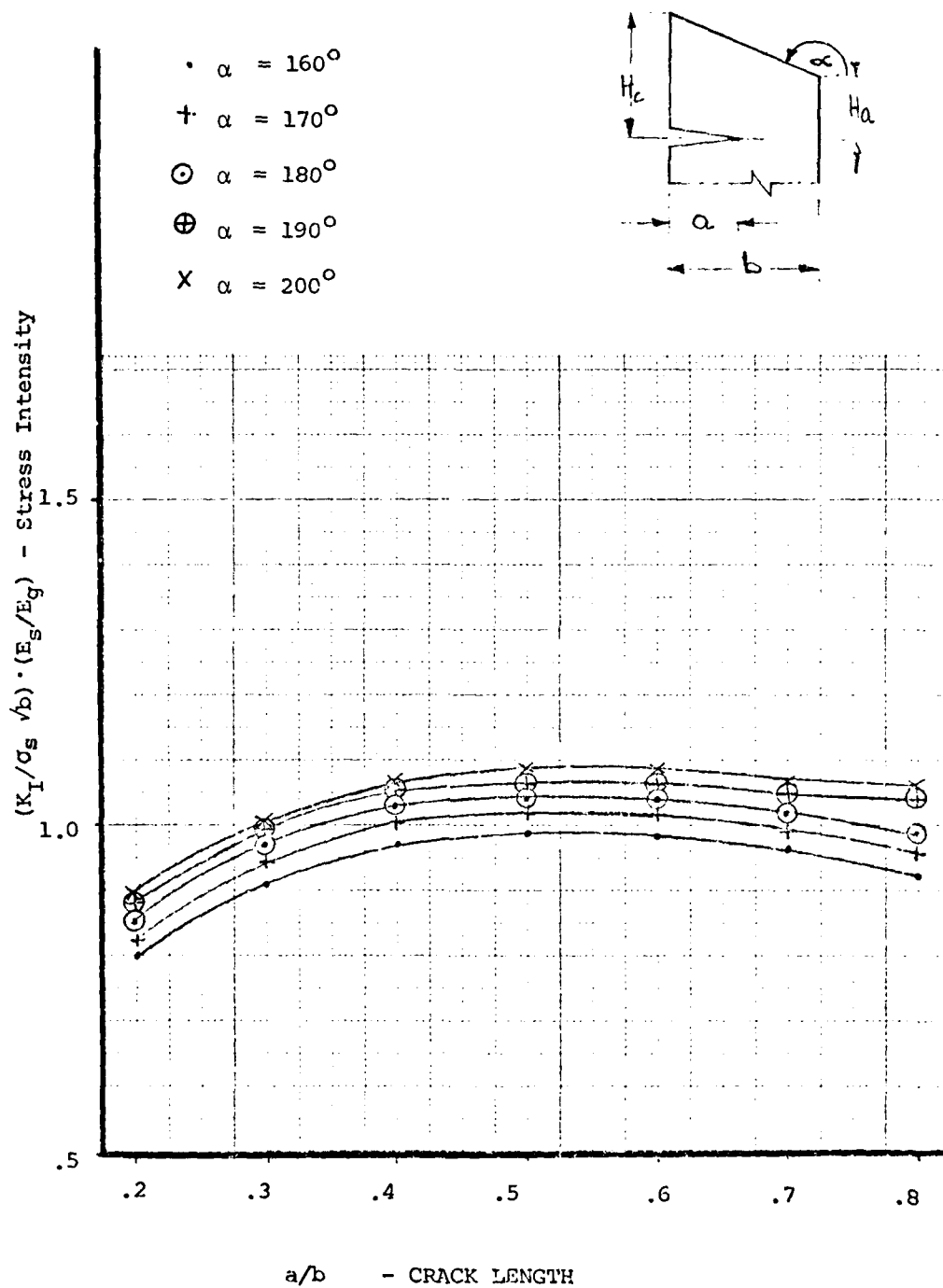


Figure 4. Stress Intensity Factor for Trapezoid Crack
Gage $H_c/b = 1$.

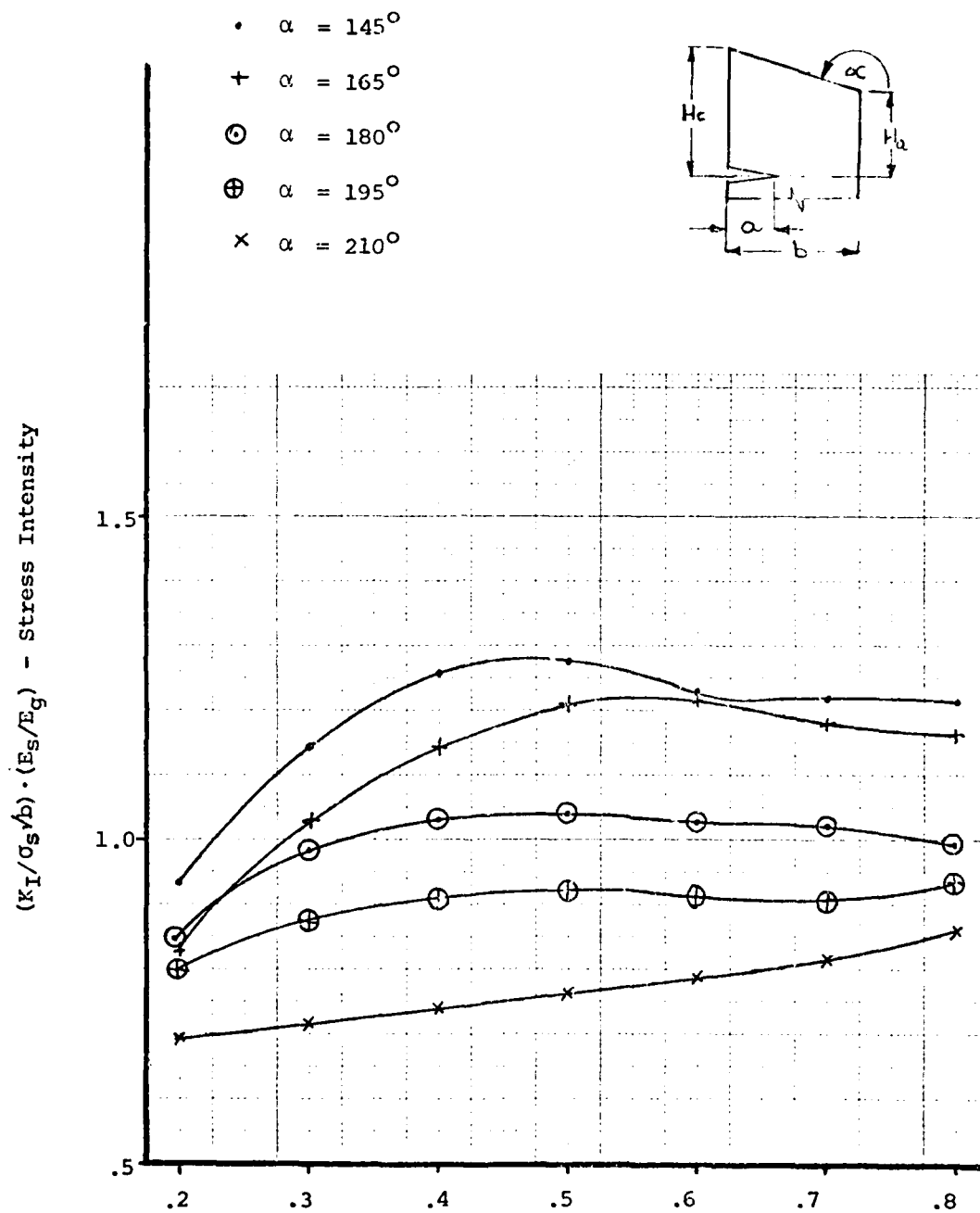


Figure 5. Stress Intensity Factor for Trapezoid Crack
Gage $H_a/b = 1$.

IV. Stress Intensity Factor Solution for a Stepped Center Crack - Crack Gage, with Prescribed End Displacements

The stepped center crack gage concept is described in Figure 6. The gage consists basically of three segments. The center segment of reduced thickness which includes the crack, and two thicker end segments.

Part of each thicker segment is bonded to the structure, and a part (of length L_0) is free. It is assumed that the gage is clamped to the structure along lines AB and GH. This assumption is only an approximation since the actual load transfer from the structure to the gage should be modeled as loads transferred through springs, where the adhesive layer is the spring element. However, the exact model was beyond the scope of this study. Displacements of line AB relative to line O-O are assumed to be transferred completely to the gage with no losses in the bond line, i.e., the bond line does not rotate.

Due to the symmetry, the center segment of the gage needs to be solved only for a quarter of the plate, as shown in Figure 7. The entire outer segment, shown in Figure 8, was analyzed in order to obtain better accuracy with the finite element analysis.

Methods of Solution

Two analytical methods will be used to obtain the complete solution. The Finite Element Method will be applied to solve forces and displacements of the outer segment of the gage and the method described in Chapter II will be used to solve for stress intensity factors, stresses and displacements for the center segment. Bowie et al (Ref 18:767-772) introduced also the idea of getting stress intensity factors by using a

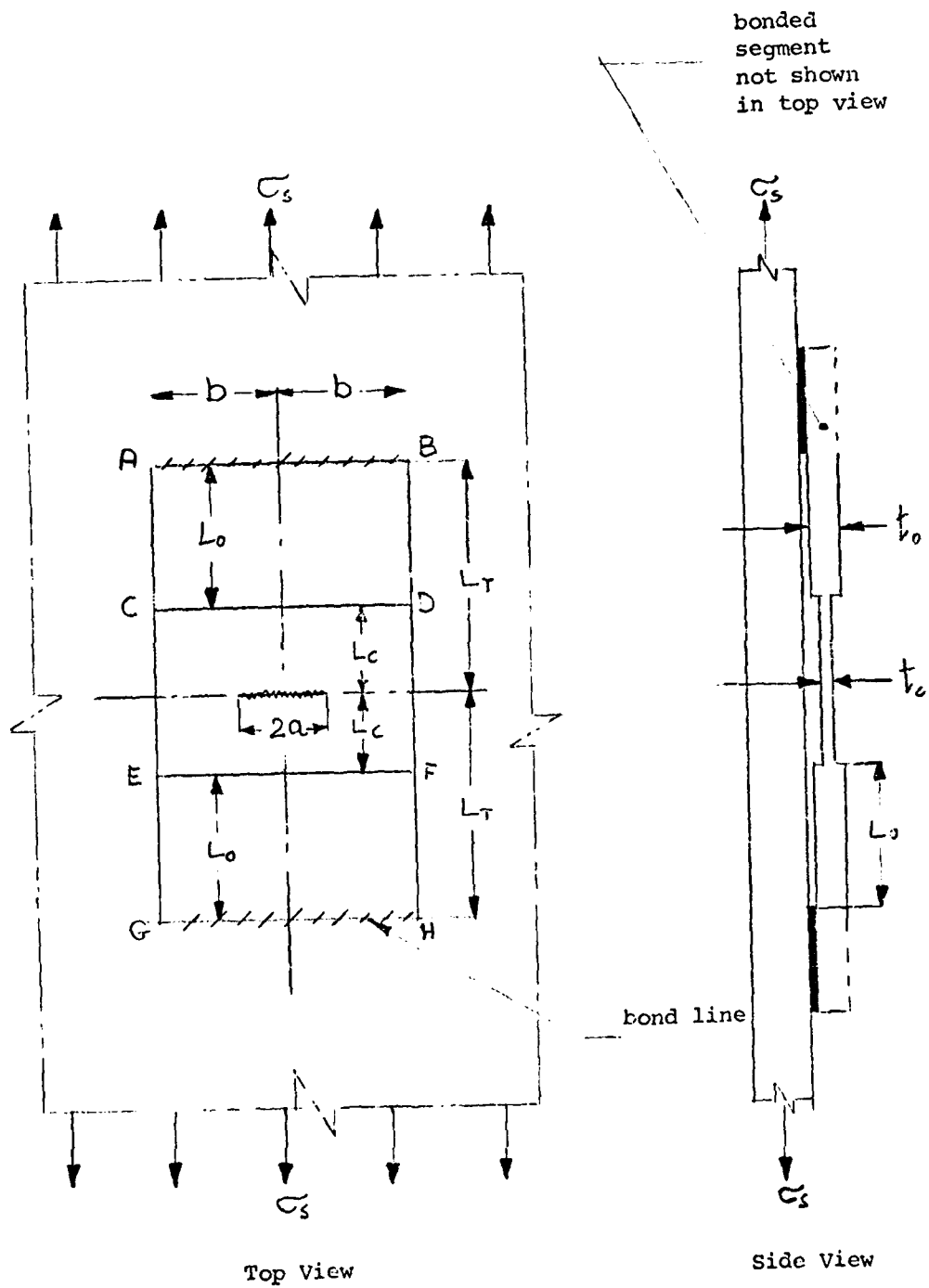


Figure 6. Center Cracked, Stepped Gage Geometry

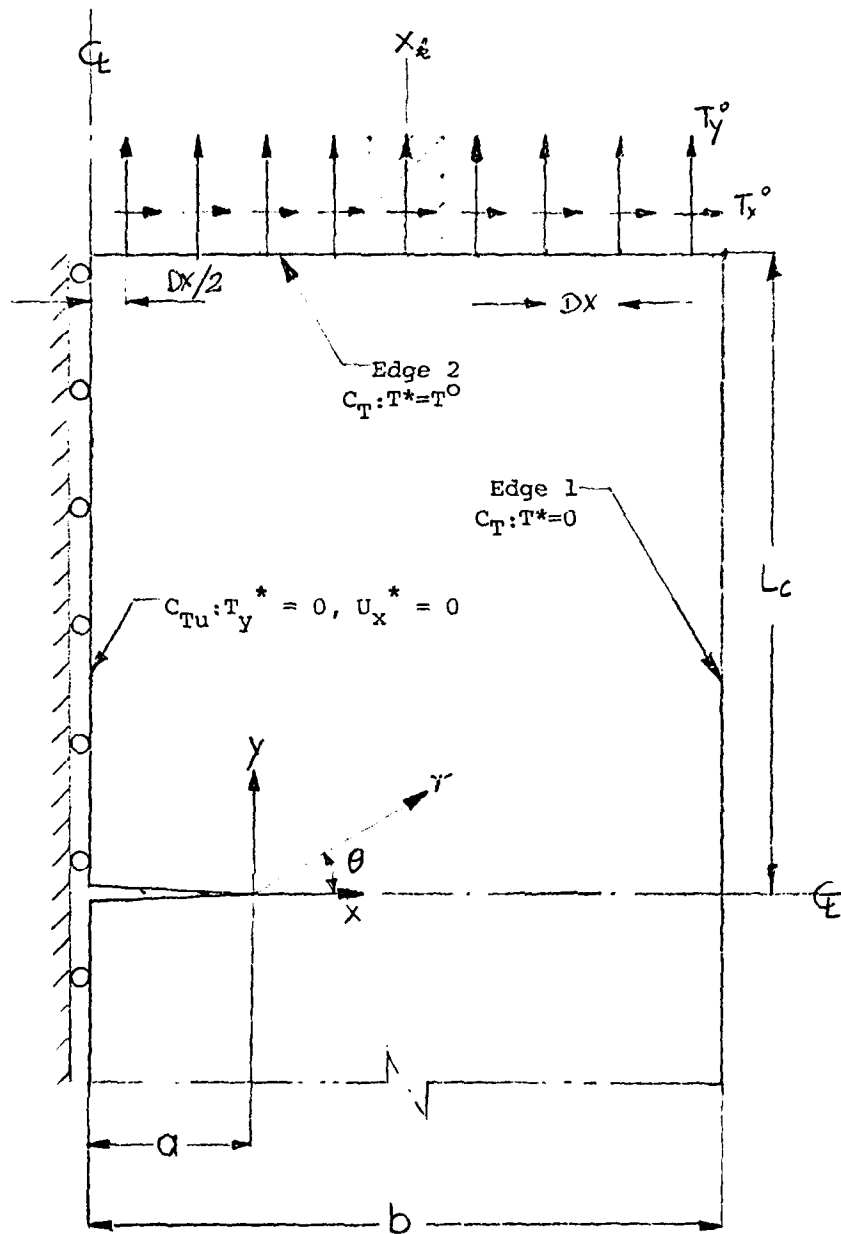


Figure 7. Center Portion of the Stepped Gage with Boundary Conditions

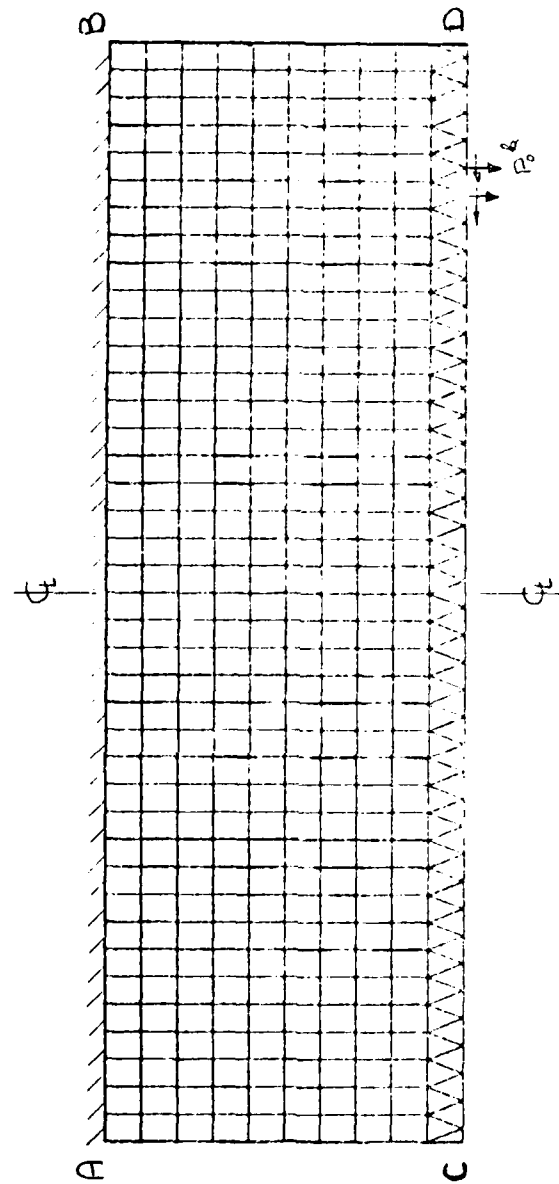


Figure 8. Stepped Gage Outer Segment

stitching technique. They used one analytical method to solve stresses and displacements for cracked and uncracked part. By stitching the solutions stress intensity factors were found for center cracked uniform thickness plate subjected to uniform stress loading.

Since the line CD is actually the connecting line between the two segments, we will demand displacements and forces produced by the two methods to be equal on this line. Let the line CD be discretized into $2n$ elements, each of length Dx . Each element will be represented by a nodal point, considered to be at the center of the segment, at which forces and displacements are assumed to be applied.

The outline for the solution is as follows:

$$\{U^*\} = \{U_C\} + \{U_O\} \quad (34)$$

where U^* , U_C are the prescribed relative displacement of line AB (Figure 6) and relative displacement of line CD with respect to inertial frame x, y , respectively. U_O is the relative displacement of line AB with respect to CD. Using flexibility matrix of center segment $[S_C]$, and flexibility matrix of outer segment $[S_O]$, we have

$$\{U_C\} = [S_C] \{P_C\} \quad (35)$$

$$\{U_O\} = [S_O] \{P_O\} \quad (36)$$

$$\text{On line CD, the forces } \{P_O\} = \{P_C\} \quad (37)$$

After substitution

$$\{U^*\} = \left[[S_O] + [S_C] \right] \{P_C\} \quad (38)$$

All the forces and displacements are expressed by x and y direction components consequently all matrices are partitioned and the number of rows or columns is twice the number of nodal points under consideration.

Suppose a unit load is applied to each element of the center segment, successively. Using the technique described in Chapter II, the coefficients of the expansion may be solved for each loading case. From the coefficients solved for a unit load at nodal point k , the first is of particular interest and will give the stress intensity factor for unit load at nodal point k . When we repeat the procedure for all nodal points, we may construct an array $\{D\}$ whose k 'th element is the contribution of load at point k to the stress intensity factor. The stress intensity factor for the center segment under uniform discretized unit load is obtained by summing the elements of $\{D\}$. If the load at each nodal point is different, the stress intensity factor solution may be written as:

$$K_I = 2\pi\{D\}^T \{P_C\} \quad (39)$$

or,

$$K_I = 2\pi\{D\}^T [[S_C] + [S_O]]^{-1} \{U^*\} \quad (40)$$

Thus, the solution for the stepped gage with prescribed end displacements requires that the flexibilities $[S_C]$ and $[S_O]$ be determined.

A prescribed stress T^* , on k 'th element, Dx long, may be converted into a "concentrated" stress at the nodal point x_k producing a unit force per unit thickness by defining a loading function.

$$T_x^* = \delta(x - x_k) \quad T_y^* = \delta(x - x_k) \quad (41)$$

so as to produce a unit force in each coordinate direction on any element, centered on x_k .

$$\int_{x_k - Dx/2}^{x_k + Dx/2} \delta(x - x_k) dx = 1 \quad (42)$$

For simplicity a unit thickness is considered. The vector F_q can be computed by Eq (30), with displacements evaluated at x_k . The matrix A_{mq} can be evaluated by Eq (24) and the system of equations can be solved for the coefficients d_m by using Eq (23). With the set of coefficients known, the actual displacements at every other nodal point l can be evaluated. By repeating the procedure for $k = 1 \dots n$, we construct the flexibility matrix $[S_c]$, along with the array $\{D\}$ which is constructed from the coefficients d_l for each of k load points. The flexibility matrix $[S_c]$ is actually factored such as to account for actual thickness ratio between center and outer segments of gage. The outer segment flexibility matrix is constructed by using "ANALYZE" (Ref 19), a finite element analysis computer program developed at the Air Force Flight Dynamics Laboratory. The matrix was established by constraining one end of the segment completely to simulate the bond line, and the other end was loaded with unit forces at discrete points.

Numerical Evaluation

The problem introduced for the center segment was solved by computer programs which are described in Appendix B. The objective of the program was to evaluate the matrix A_{mq} , given in Eq (29), to solve Eq (23) for the coefficients, and to construct the flexibility matrix $[S_c]$ in the manner previously described.

The matrix A_{mq} was evaluated by a numerical integration along edges 1, 2, 3, using Simpson's third rule. The boundary was divided into 300-400 points. A slight sensitivity to the number of integration points was observed (for short, L_c) when elements of different lengths were used to perform the integration on separate edges.

The number of terms, M , used for the expansion was 18. The number of nodal points used on edge 2 was 20. Consequently, the flexibility matrixes were dimensioned 40×40 , partitioned into x and y components.

The flexibility matrix of the outer segment was developed for a whole outer plate, and the corresponding 40×40 matrix, $[S_o]$, was extracted.

The prescribed displacement U^* was chosen to be 1 in longitudinal y direction and zero in x direction. As has been shown, releasing the transverse constraints would have little effect on results (Ref 9: 32, 10), since the stress intensity factor is driven primarily by displacements perpendicular to crack plane.

Stress intensity factors were computed for center segments having lengths:

$$L_c = .4; .6; .8; 1.0; 1.25$$

The outer segments having lengths

$$L_o = 1.0; 1.267; 1.6; 2.0; 4.0$$

and for the thickness ratios

$$t_c/t_o = .2; .5; .75$$

The width in all cases was taken to be $b=2.0$.

Stress intensity factors were not calculated for all combinations of variables.

Results and Discussion

A sample of the results of a convergence study for the stress intensity factor solution of the center segment with 12, 18 and 24 terms is presented in Table I. No significant changes for more than 18 terms were observed. The number of nodal points N , was varied through

10, 20, 30, 40 and results for stress intensity factors are compared in Table II for $a/b = .2; .6$. A rapid convergence may be observed for $n > 10$. Using results for 40 nodes as a reference, 10 nodal points give about 63%, and 20 nodal points give 94% of the reference value for $a/b = .2$. For $a/b = .6$ the results for $n = 20$ is 98% of the result obtained using $n = 30$. The convergence for longer cracks seems to be better, since the relative error of load fraction distributed over the crack (governed by element size) is smaller for long cracks.

The stress intensity factor solution obtained for the uniform discretized stress loading on the central segment is given in Table III, and is compared to published results for a uniform stress loading (Ref 20:11). Table III shows that present results are low by five percent, a factor that may be attributed to the number of nodal points.

In order to check the overall approach, cases of $t_c/t_o = 1$ were run. This case is actually a case of a center crack gage with uniform thickness and half length of $L_c + L_o$, subjected to prescribed displacements at the end. Comparison to published results (Ref 20:16) indicated that present results are within 10-15% higher than published for the same aspect, ratios, and uniform thickness.

Due to the fact that the gage is constructed from relatively short plates, the finite elements solution was checked thoroughly, and results were found reasonable (see Appendix C). However, the finite element analysis was performed on a complete outer segment instead of a half since the displacements results were more reasonable in this configuration.

During the center segment analysis, attempts to invert the flexibility matrix were made and difficulties encountered. However, no

Table I
Convergence of Stress Intensity Factor
 $K_I/\sigma_s\sqrt{b}$

$L_c = .4$	$b = 2.0$	$n = 20$
<u>$M^{**} = 12$</u>	<u>$M = 18$</u>	<u>$M \approx 24$</u>
1.2620	1.2660	1.2662

*n = number of nodal points on half width

**M = number of terms in expansion

2M = number of coefficients in expansion

Table II
Convergence of Stress Intensity Factor
 $K_I/\sigma_s\sqrt{b}$

<hr/>				
$L_C = .4$	$b = 2.0$		$M = 18$	
<u>a/b</u>	<u>n = 10</u>	<u>n = 20</u>	<u>n = 30</u>	<u>n = 40</u>
.2	.8497	1.266	1.322	1.30
.6		6.607	6.731	

Table III
Stress Intensity Factor for Stress Loading - Comparison
with Published Results

a/b	$L_c/b = .5$ $K_I/\sigma_s \sqrt{b}$ Present Results Discrete load	Rooke (Ref 20) (Data transferred to same nondimensional form)
.2	.84	.88
.4	1.70	1.78
.6	3.15	3.28

explanation for this difficulty was found. The final results, as well as the intermediate results of the analysis, were within reasonable agreement with other published results. Thus, the flexibility matrix was accepted in spite of the unexplained difficulty in computing an inverse.

Figures 9 through 19 show the stress intensity factor results obtained in this study. One of the gages ($L_c/b = .2$ $L_o/b = .63$ $t_c/t_o = .5$) was developed by McDonnell Douglas Corporation as part of the evaluation of the crack gage on F-4 full scale fatigue test (Ref 14). Another gage ($L_c/b = .625$ $L_o/b = .625$ $t_c/t_o = .2$) was developed by Boeing Wichita as part of contract F33615-77-C-5073 (Ref 13). The results are given in a nondimensionalized form ($K_I/\sigma_s \sqrt{b}$) (E_s/E_g) vs. a/b , where σ_s is the stress of the carrying structure at the bond line, such that a longitudinal displacement

$$U^* = \frac{\sigma_s}{E} L_T \quad (43)$$

is transferred to the gage, b is the width of the gage and a is the length of the crack. Figure 9 shows the typical benefits of the stepped gage compared to a gage with uniform thickness. For the same aspect ratio, i.e., 1.5, the stepped gage gives a 40% higher stress intensity factor and is more constant. Furthermore, the range of stress intensity factor available to choose for a specific need with geometrical restrictions is very large. Figures 10 through 18 show that stress intensity factor will grow as thickness ratio will decrease, and as L_o grows for a given L_c . Figure 19 is typical, showing the effect of change in thickness ratio change while the length ratio is held fixed. It may be observed that changes in length ratios of center and outer segment appear to change the magnitude and the shape of SIF vs. a/b , while thickness changes will affect primarily the magnitude only. It was found that for a thickness ratio less than $t_c/t_o = .1$, the stress intensity solution is as if the prescribed displacement was applied directly to the center segment.

For fast approximations of the stress intensity factor, the following equation may be used (see Appendix D for details).

$$\frac{K_I}{\sigma_s \sqrt{b}} \left(\frac{E_s}{E_g} \right) = \frac{L_o + L_c}{\sqrt{b} \left[\sqrt{\frac{8}{\pi}} \cdot \frac{L_o}{b} \cdot \frac{t_c}{t_o} \sqrt{b-a} + \sqrt{(1-\nu^2)L_c} \right]} \quad (44)$$

In this equation, Rice's (Ref 22) limit values for K_I in a short infinite strip with a semi-infinite crack is encountered. The values of K_I obtained by this approximation are within 10-15% lower than the actual solution, for $a/b > .6$. The approximation was verified for values of t_c/t_o and L_c/L_o in the range investigated, and is suggested as a rapid means of obtaining a trial design with desired stress intensity factor.

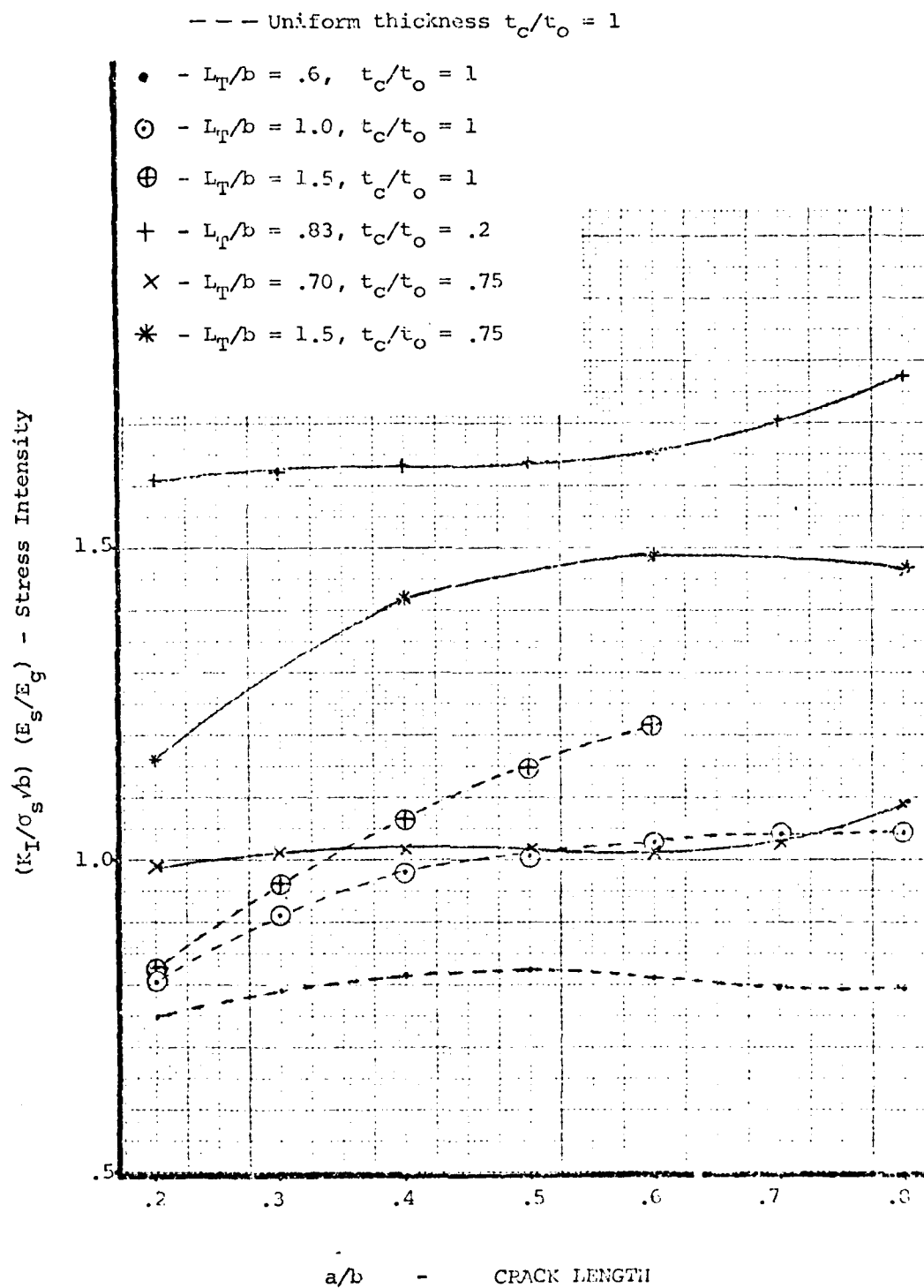


Figure 9. Comparison of Stress Intensity Values for Center Cracked Uniform Thickness Gage and Stepped Gage

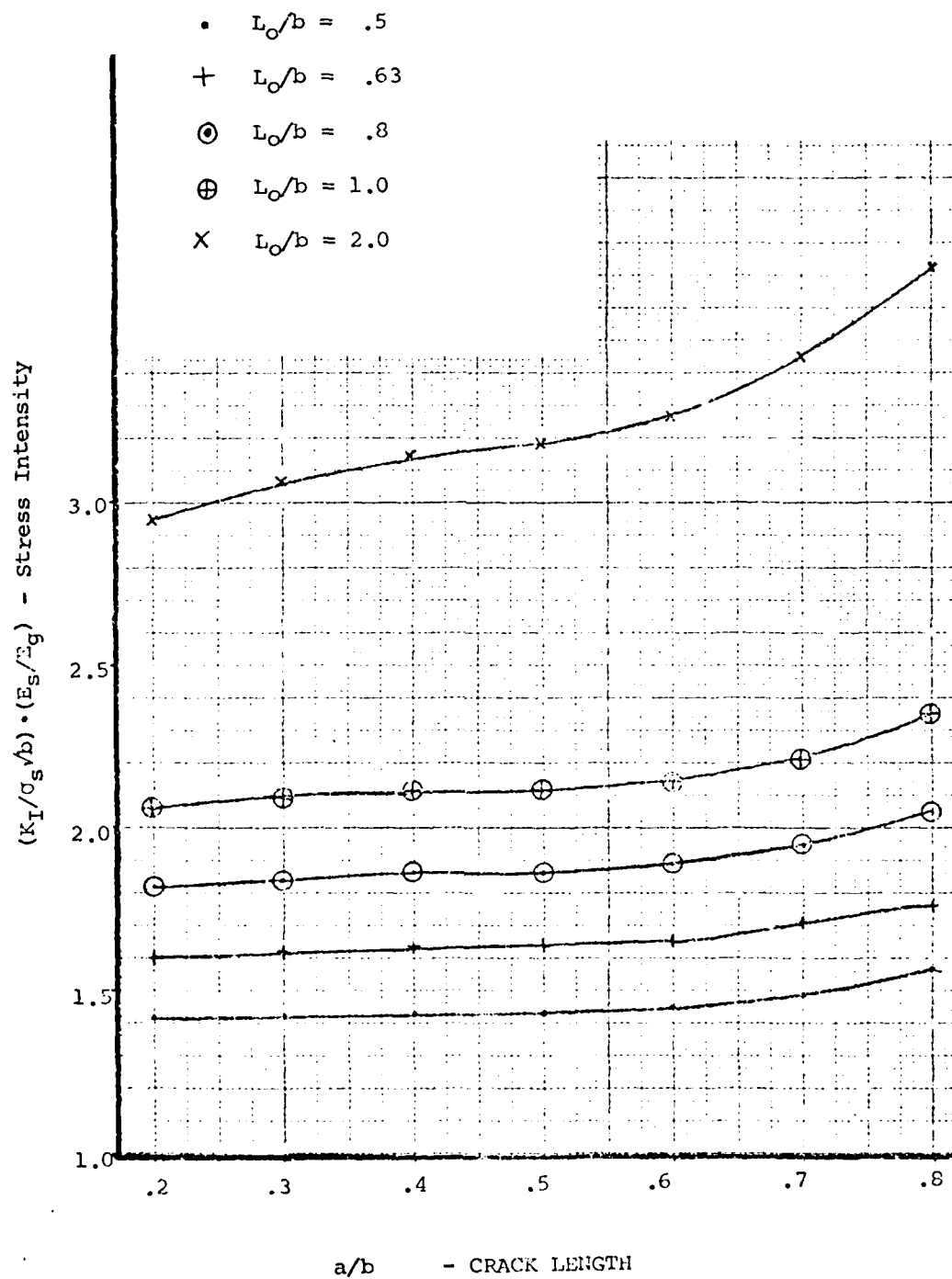


Figure 10. Stress Intensity Factor Results for Gage
with $t_c/t_o = .2$, $L_o/b = .2$

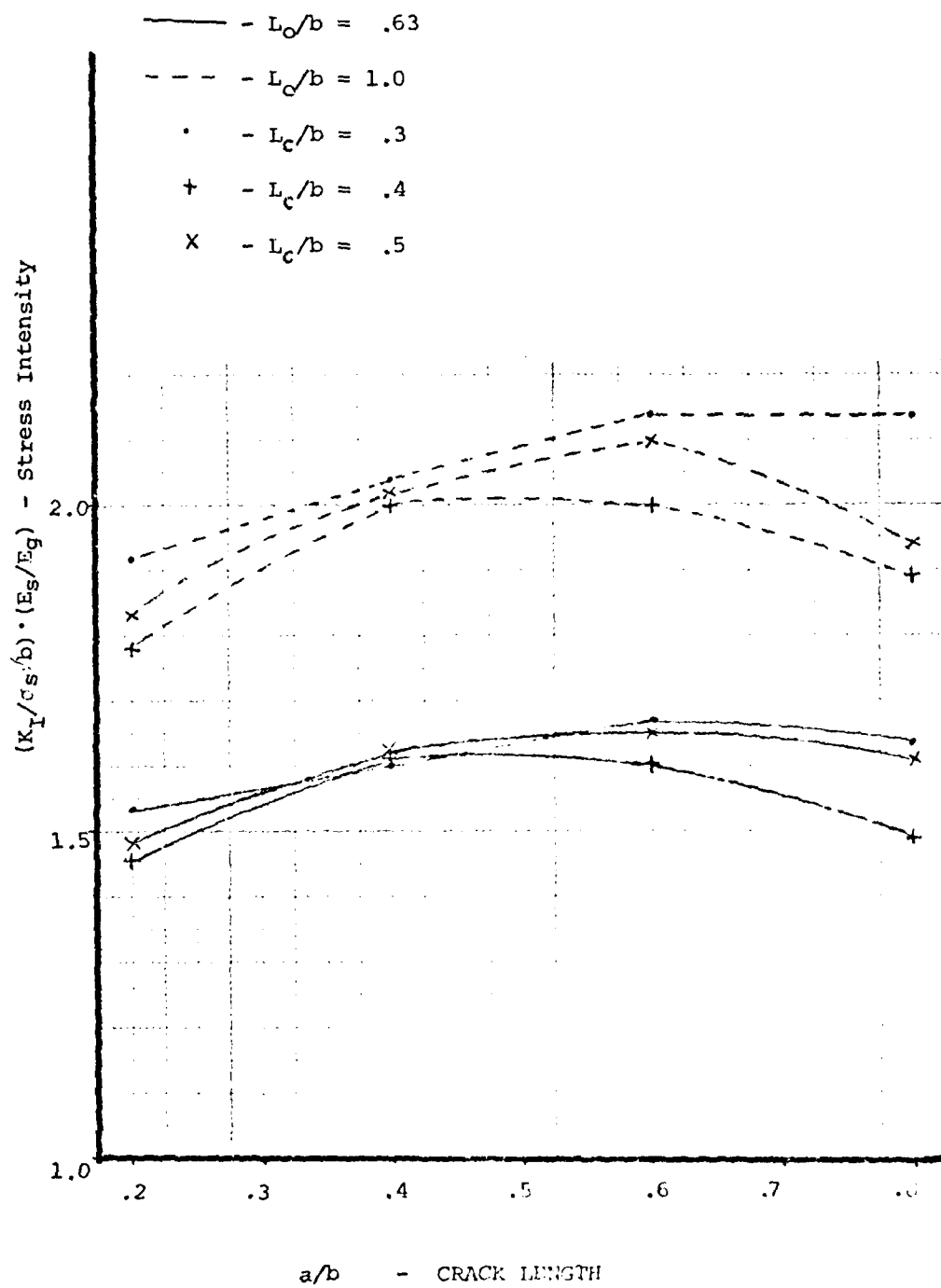


Figure 11. Stress Intensity Factor Results for Gage with $t_c/t_o = .2$, Various Length Ratios

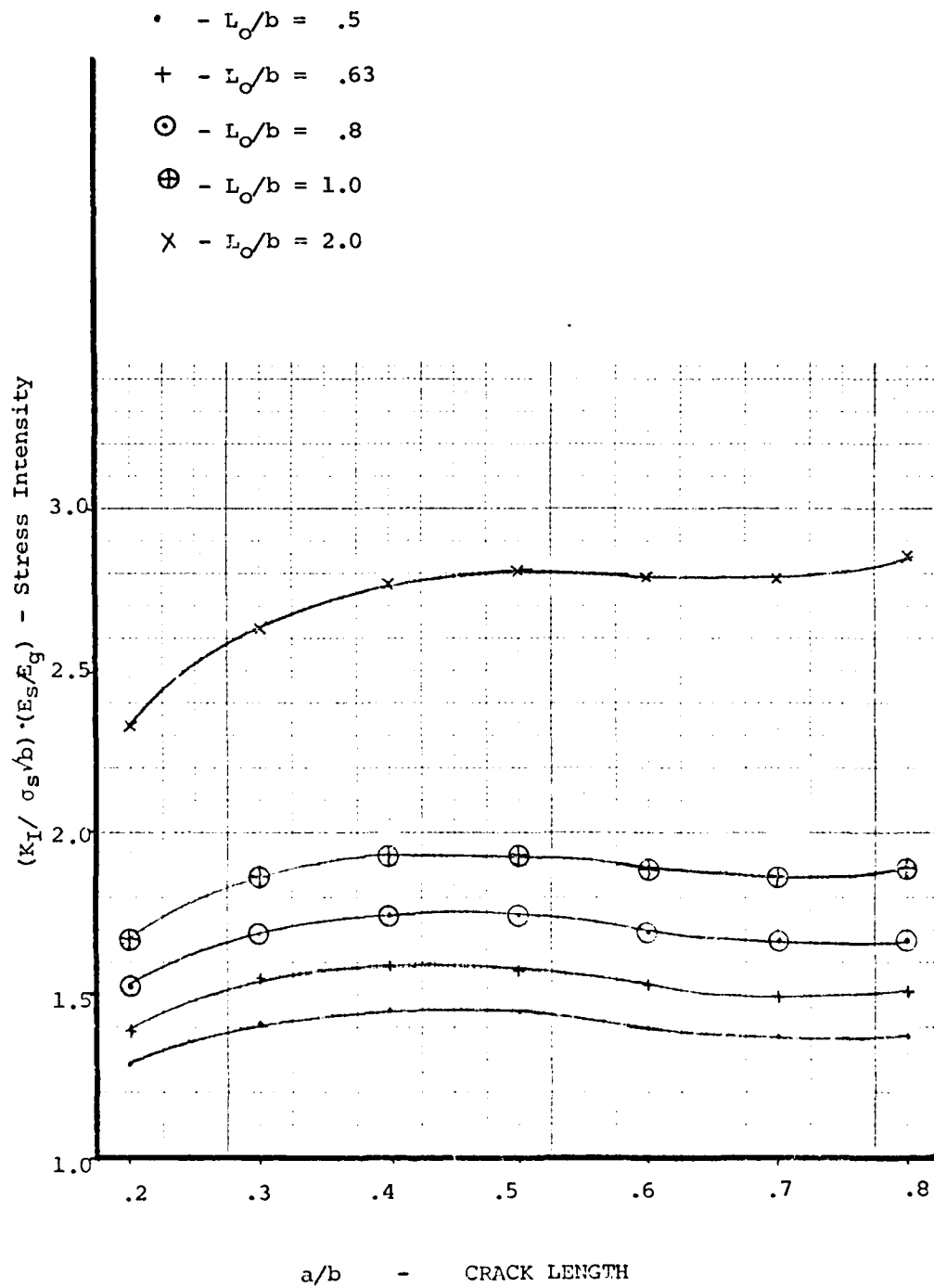


Figure 12. Stress Intensity Factor Results for Gage
with $t_c/t_o = .2$, $L_c/b = .625$

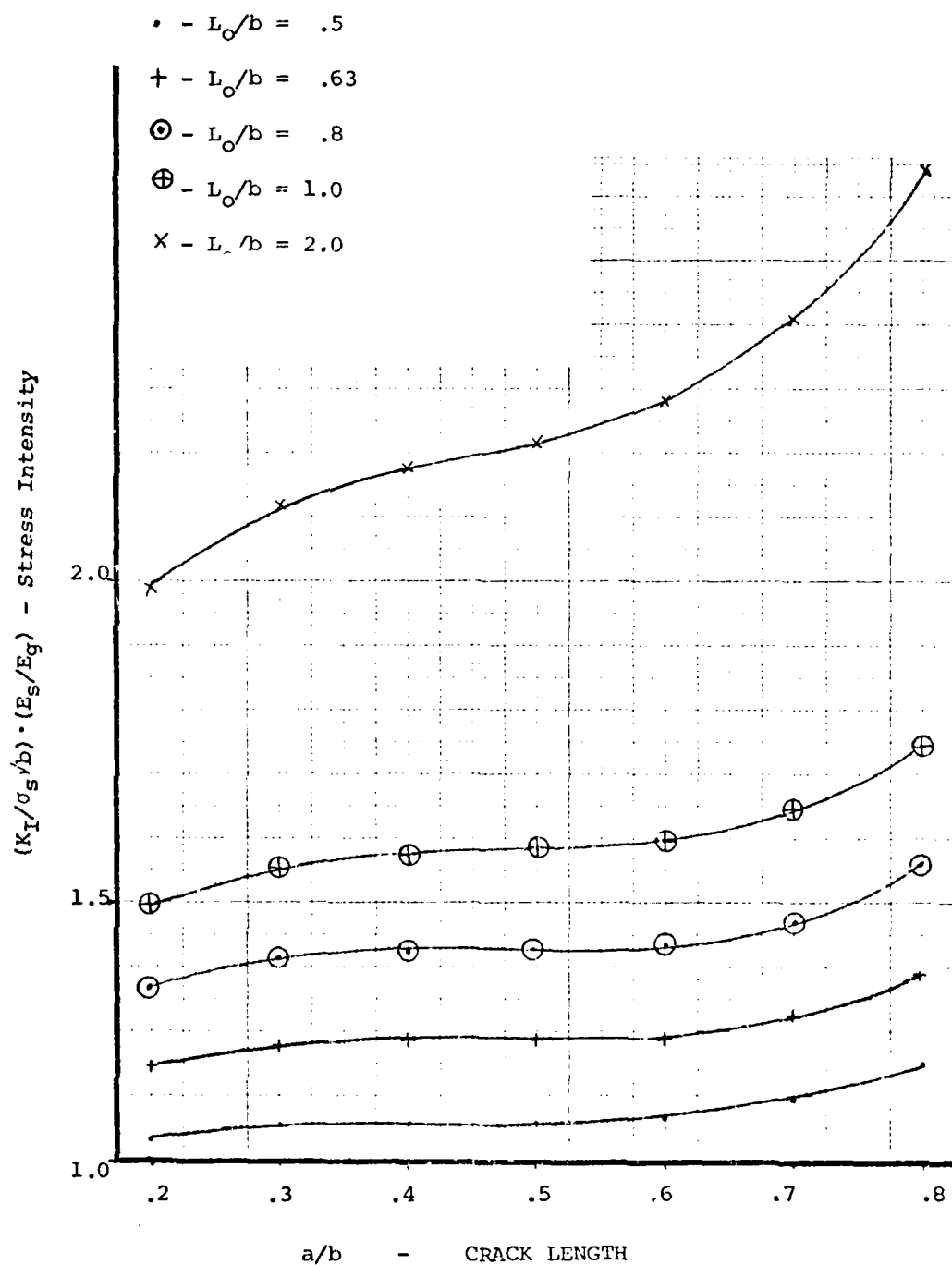


Figure 13. Stress Intensity Factor Results for Gages
with $t_c/t_o = .5$, $L_o/b = .2$

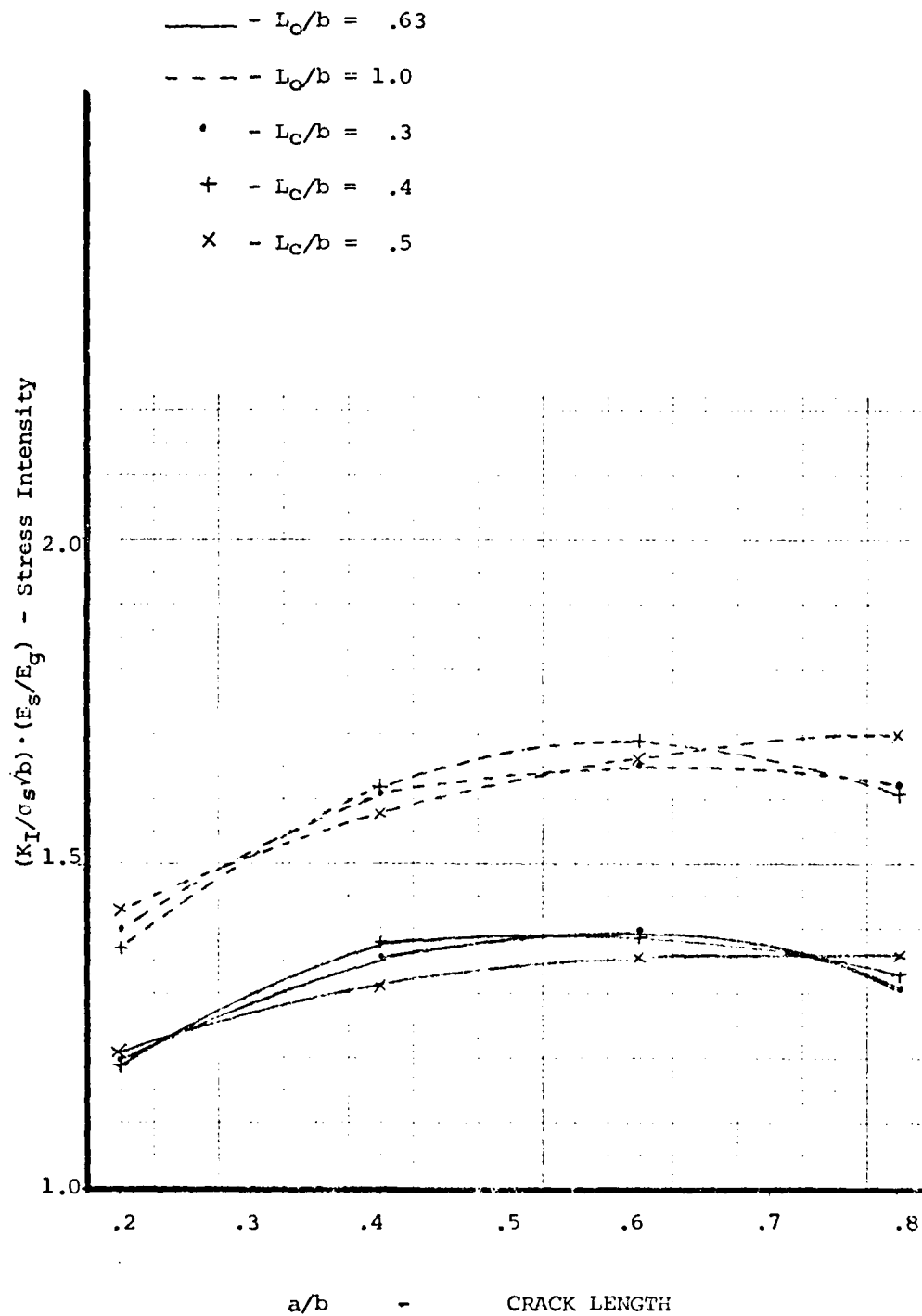


Figure 14. Stress Intensity Factor Results for Gages with $t_C/t_O = .5$, Various Length Ratio

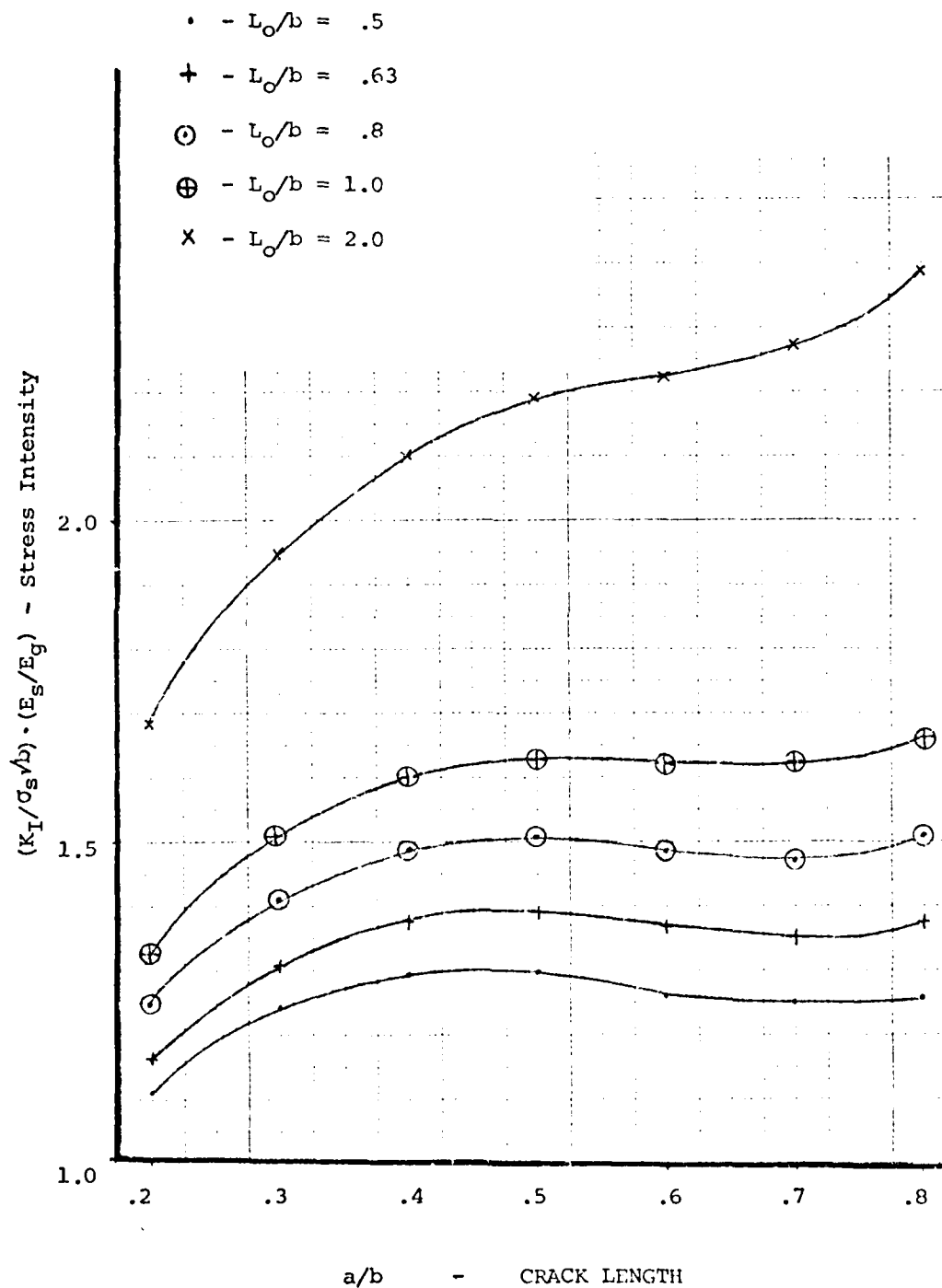


Figure 15. Stress Intensity Factor Results for Gage
with $t_c/t_o = .5$, $L_c/b = .625$

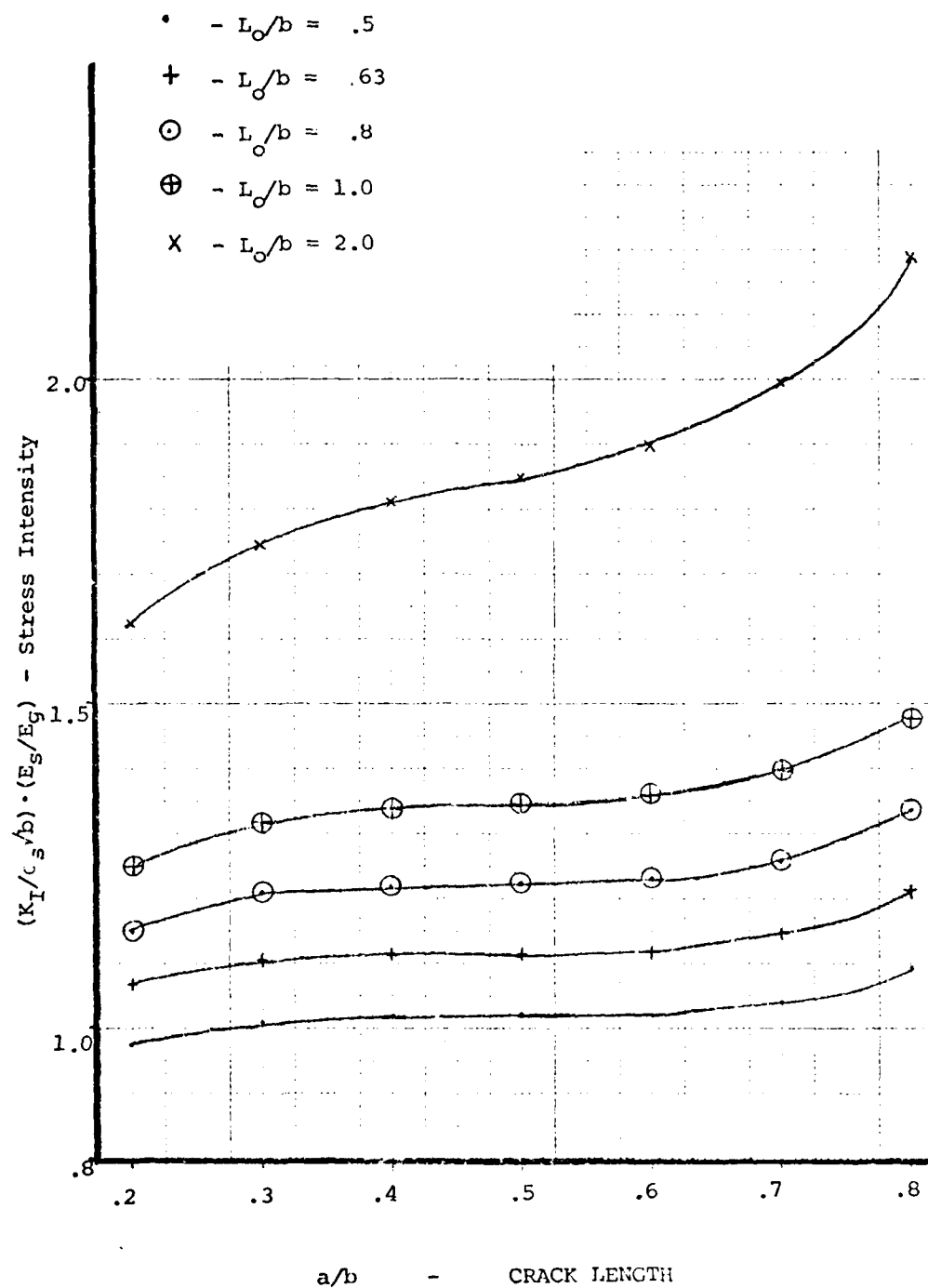


Figure 16. Stress Intensity Factor Results for Gages
with $t_c/t_o = .75$, $L_c/b = .2$

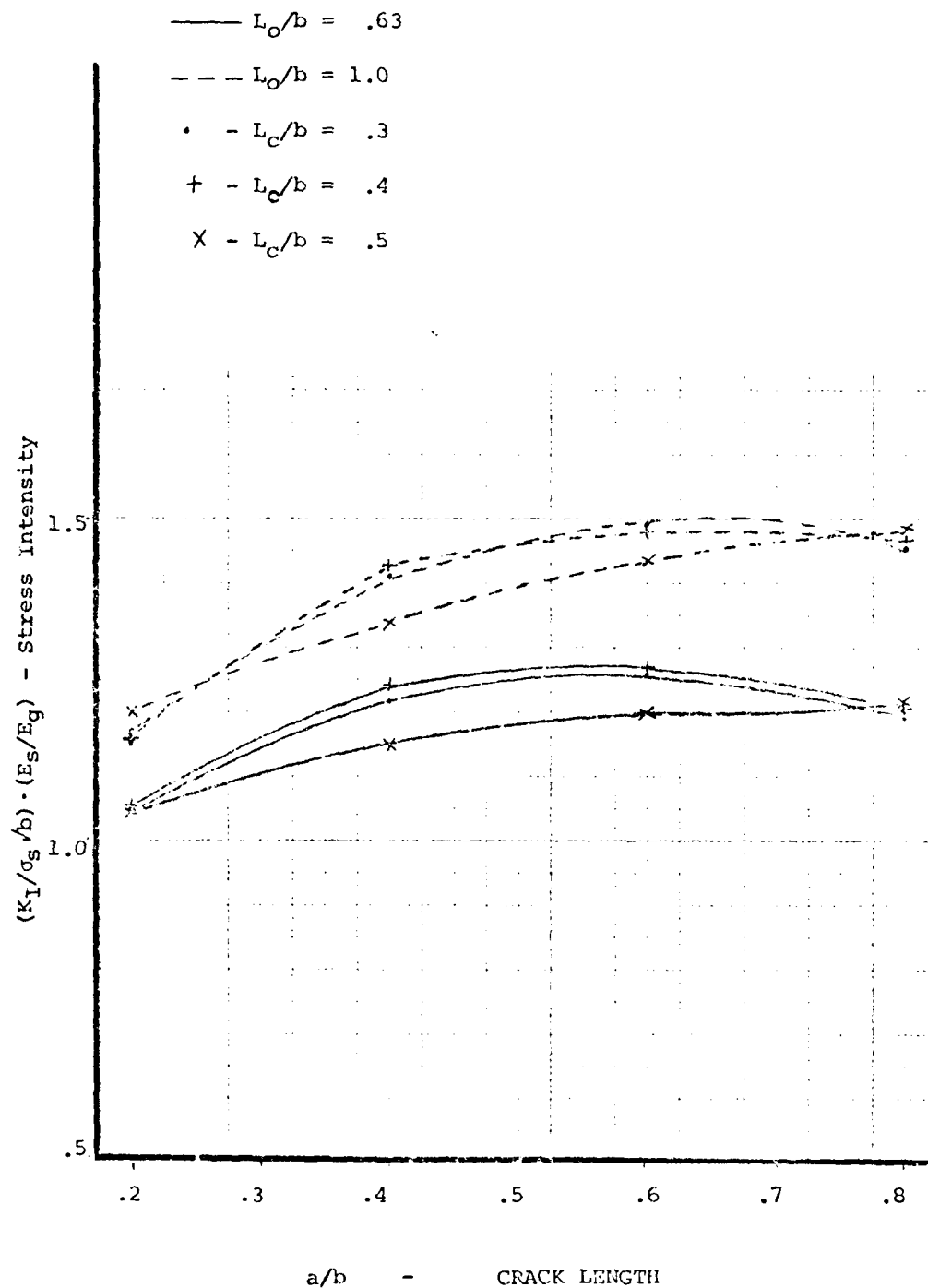


Figure 17. Stress Intensity Factor Results for Gages with $t_c/t_o = .75$, Various Length Ratios

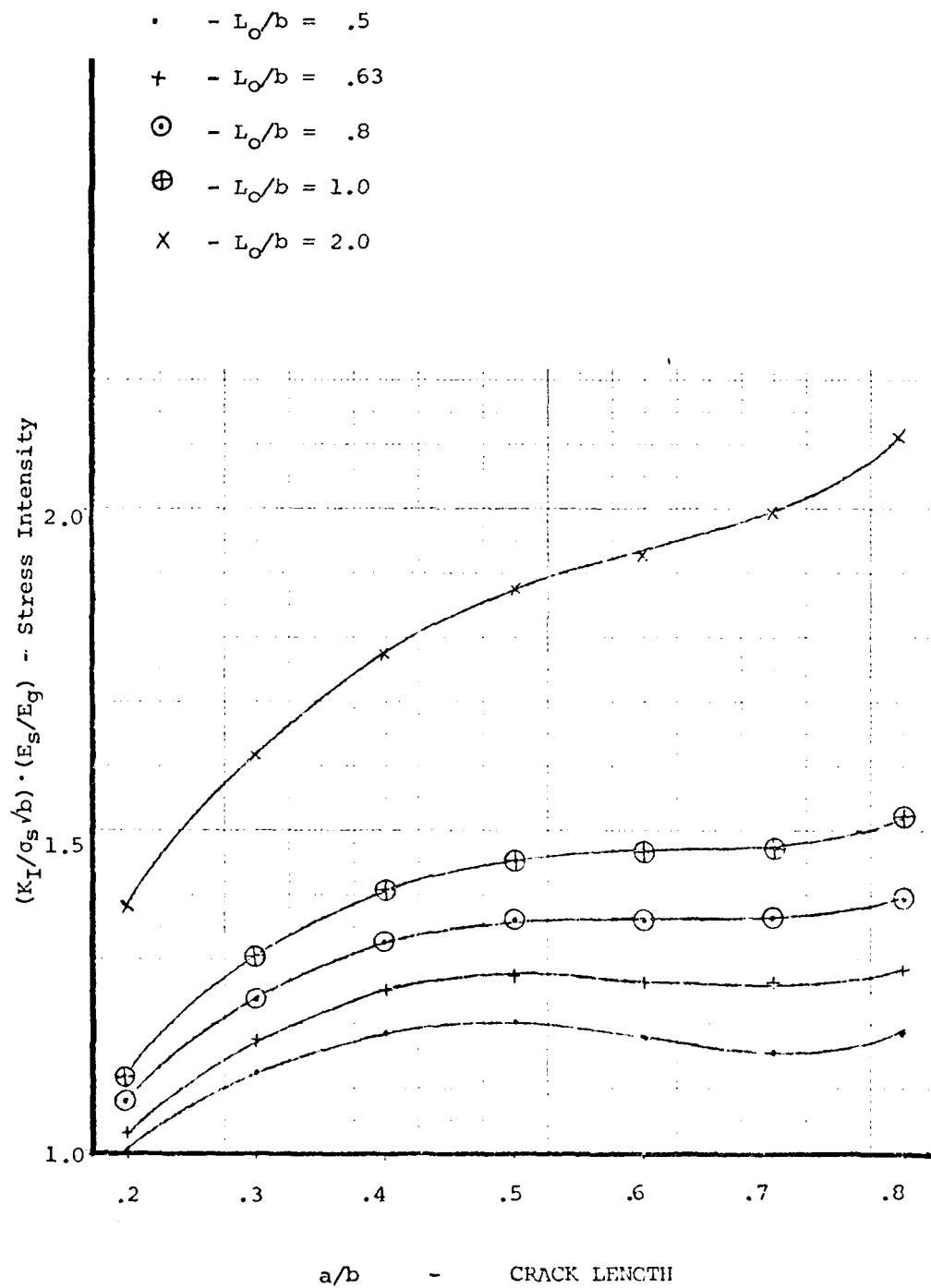


Figure 18. Stress Intensity Factor Results for Gages
with $t_c/t_0 = .75$, $L_0/b = .625$

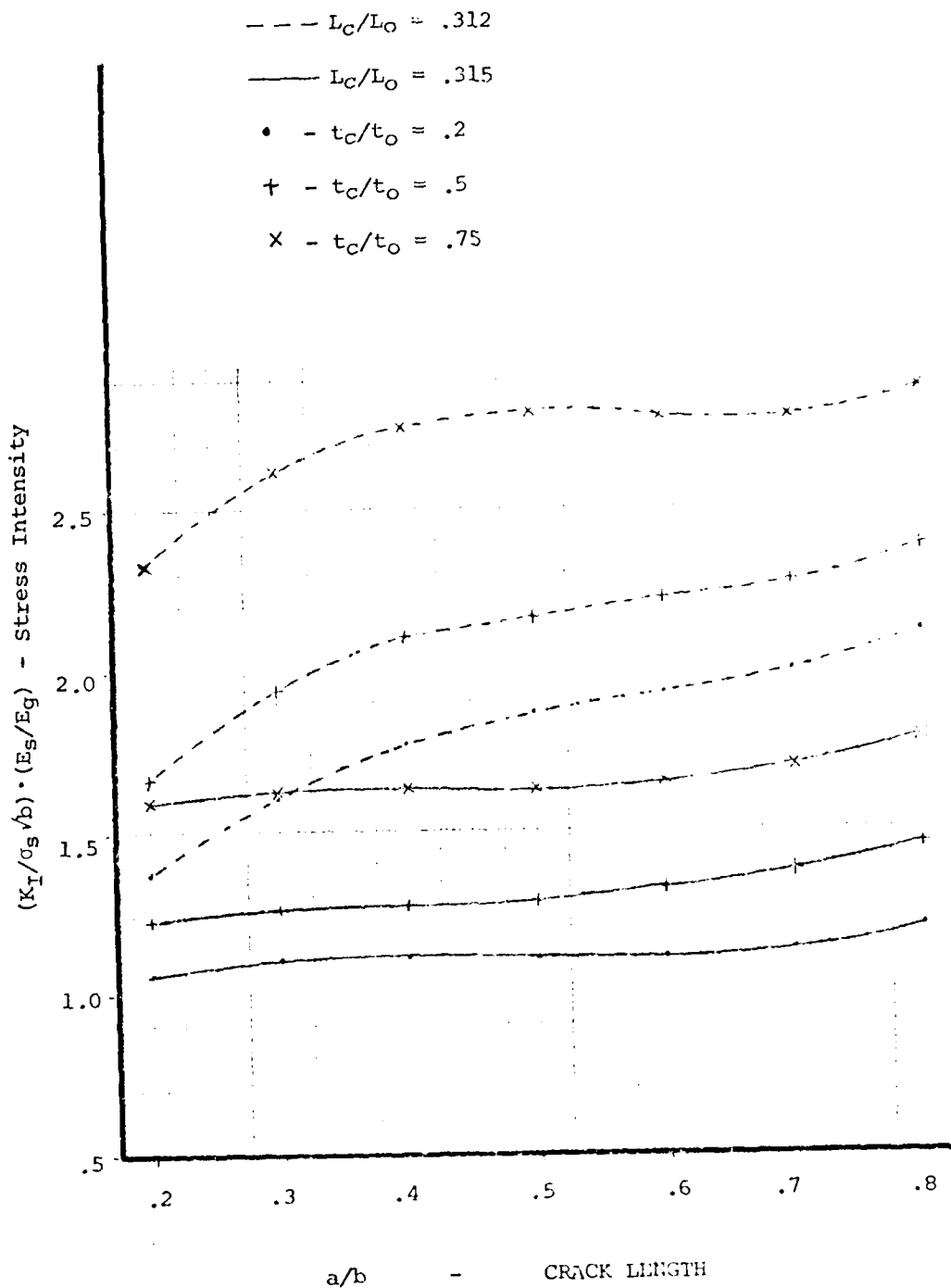


Figure 19. Stress Intensity Factor Results for
 $L_C/L_O = .315$ $L_C/L_O = .312$

V. Experimental Results

The methodology for the verification of analytical results of stress intensity factor for center cracked stepped gage is based on Paris' law.

$$da/dN = C(\Delta K)^m \quad (45)$$

Where a is the crack length; N the number of loading cycles; C , m the material constants and ΔK is the difference of stress intensity factor for each loading cycle. If we measure da/dN in an experiment, we can find ΔK , provided the material constants C and m are known. When conducting a constant amplitude stress cyclic test with $R=0$ where R is $\sigma_{min}/\sigma_{max}$, then ΔK becomes actually the stress intensity factor. This sort of test is to be designed such that no retardation effects will be experienced during the test. A series of experiments were designed to check the analytical results of this study and in addition were a part of the evaluation of the crack gage designed by McDonnell Douglas for the F-4 full scale fatigue test. Due to technical difficulties, this test program is not completed and intermediate results are not reported. However, Boeing (Wichita) as part of contract No. F33615-77-C-5073 (Ref 13) has conducted a series of base line tests and constant amplitude stress crack growth test for a similar stepped crack gage. Since their data was applicable for verification of the results presented in this study, raw data was obtained and reduced to compare to analytical results to be presented.

The material used for the Boeing specimens was 7075-T651 aluminum. The Paris' law constants were found to be $C = .1479 \times 10^{-14}$ and $m = 2.49145$

where the units of da/dN and ΔK are in/cycle and $\text{psi}\sqrt{\text{in}}$, respectively. base line data was fit to equation (45) with a computer program provided by Dr. Ashbaugh and Dr. Grandt from AFML (Ref 23). This program uses Feddersen's formula modified by Tada (Ref 21:2.2) to evaluate K_I for a center crack coupon. The gage shown on Figure 20, was bonded to the carrying specimen, shown in Figure 21, by FM-73 adhesive. Constant load amplitude tests were conducted with $\sigma_s = 10,000$ psi and $R = 0$. Crack growth vs. cycles was recorded. From a vs. N data, da/dN was calculated and by applying Paris' law, K_I was determined. The results shown in Figure 22 were taken from two different tests employing six gages, and where gages were located back to back on the carrying specimen. The first test carrying specimen, AFCG-1, included two of the gages. On the second test specimen, AFCG05, four gages were bonded to the carrying specimen. The graphical results of Figure 22 show very good agreement between test and prediction. It has to be noted that there is significant scatter in the experimental results, as is to be expected. Scatter is inherent in this experimental procedure due to variation in materials, loading accuracy, crack length reading and differentiating procedure used to obtain da/dN .

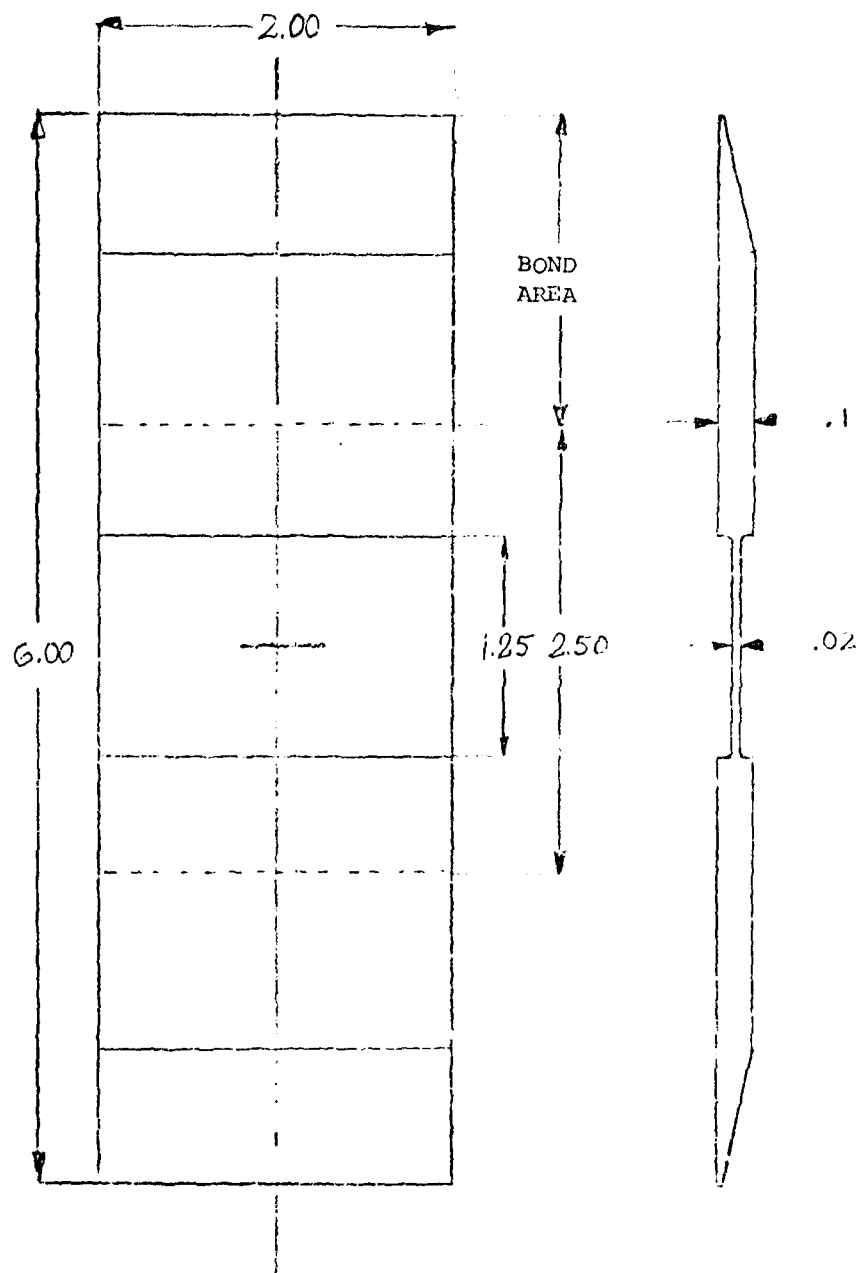


Figure 20. Tested Stepped Gage Schematic Geometry

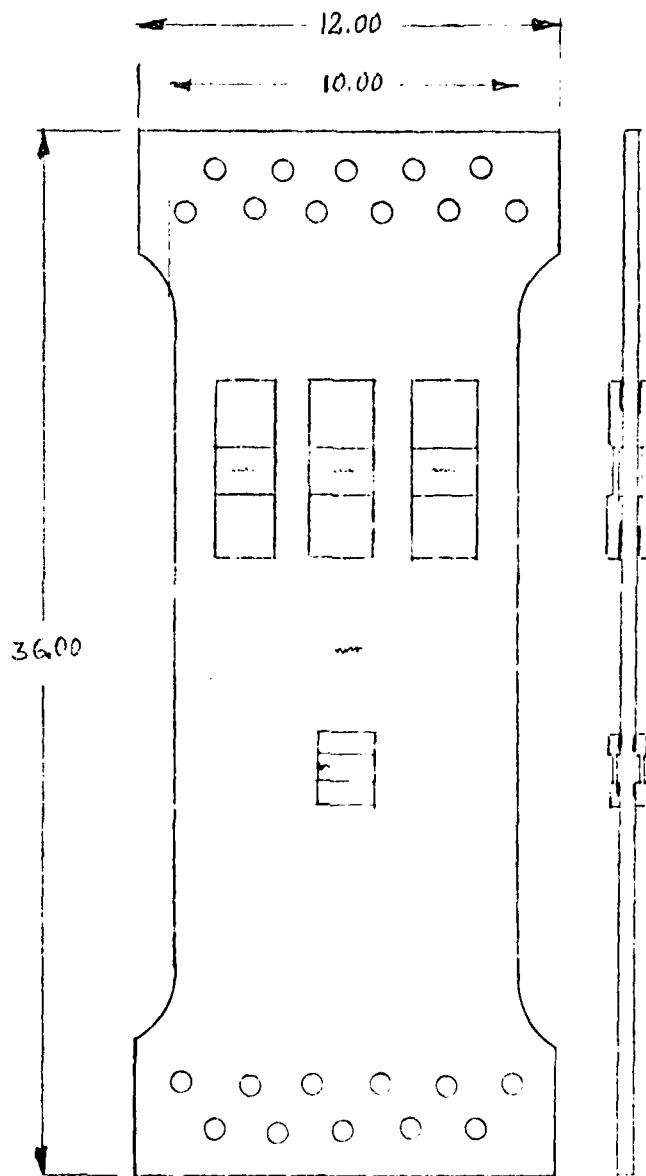


Figure 21. Carrying Specimen with Typical Crack
Gage Arrangement

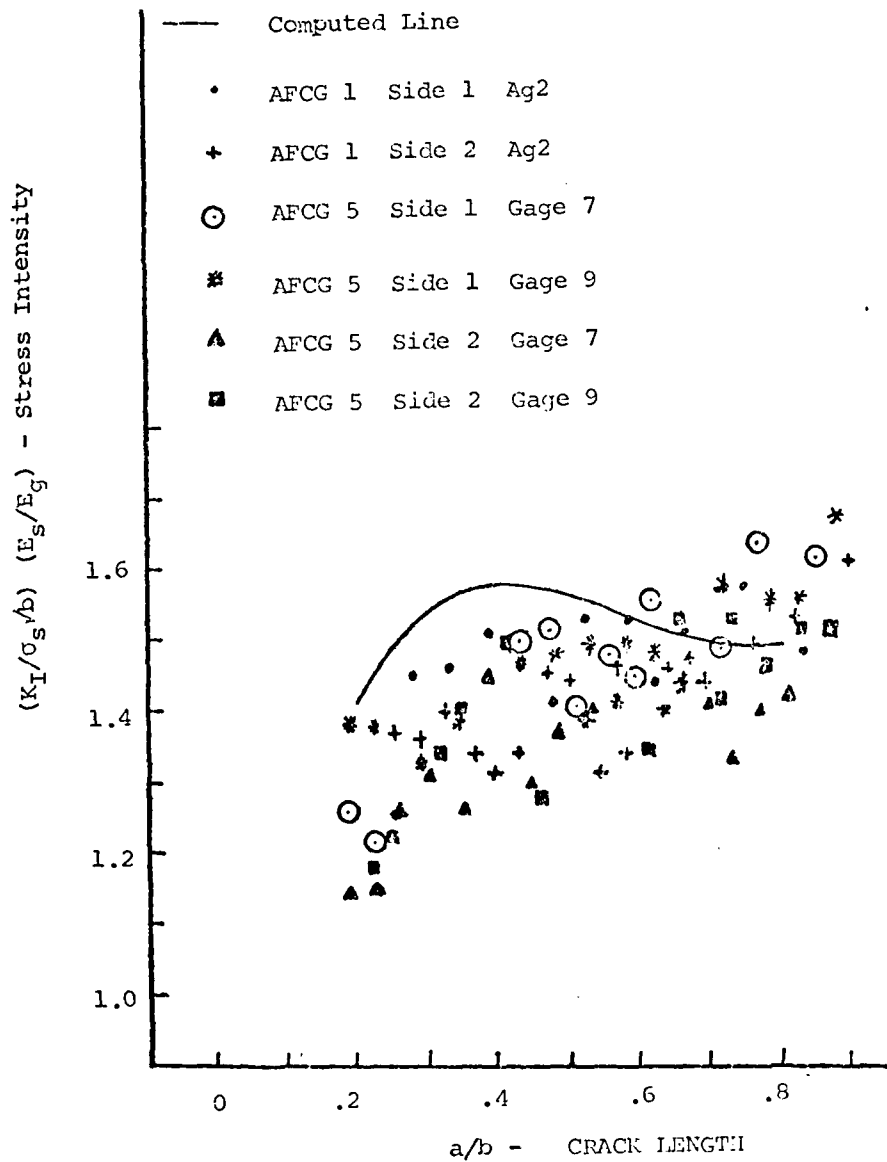


Figure 22. Comparison Between Calculated Stress Intensity Factor and Experimental Results
Gage Dimensions $t_c/t_o=.2$, $L_c/L_o=1.0$

VI. Conclusions and Recommendations

This study provided methods for obtaining stress intensity factors for trapezoidal planform gage and stepped gages. For the stepped gage solution, a method was developed using Reissner's principle along with finite element techniques which proved to give satisfactory results, as verified by test. It was clearly demonstrated that the stepped gage can be designed to have stress intensity factors within a wide range.

Conclusions

1. The trapezoid shaped edge cracked gage has no significant advantage over rectangular gages.
2. The method of solution introduced for stepped gages has been shown to be suited to the analysis of these geometries with good accuracy.
3. The stepped center crack gage provides a convenient means for obtaining desired stress intensity factors due to the relative ease with which substantial changes in K_I may be obtained by varying the geometry, and is to be preferred to other geometric shapes which have been considered for the crack gage.

Recommendations

1. It is recommended that the analytical results presented in this study be verified by further testing of stepped gages of other geometries.
2. It is recommended that the K_I solution method for stepped gages introduced be included in crack growth prediction models so as

to provide an analytical model for crack growth prediction for crack gages under load sequence more complicated than constant amplitude.

Bibliography

1. Coffin and Tiffany, C. F. "New Air Force Requirements for Structural Safety, Durability and Life Management," Journal of Aircraft, Vol. 13, February 1976, pp. 93-98.
2. Aircraft Structural Integrity Program Requirements. Washington: Department of Defense, 11 December 1975. MIL-STD-1530A(11).
3. F/RF-4C/D Damage Tolerance and Life Assessment Study, Vol. 1. St. Louis, Missouri: McDonnell Douglas Corporation, February 1975. MDC-A2883.
4. Model F-4E Slatted Airplane Fatigue and Damage Tolerance Assessment, Vol. 1, McDonnell Aircraft Co., July 1975. MCD A3340.
5. Pinckert, R. E. "Damage Tolerance Assessment of F-4 Aircraft." AIAA paper 76-904 presented at the Aircraft Systems and Technology Meeting, Dallas, Texas, on September 27-29, 1976.
6. Gray, T. D. and A. F. Grandt. "An Evaluation of the Crack Gage Technique for Individual Aircraft Tracking." Proceedings of Army Symposium on Solid Mechanics, 1978 Case Studies on Structural Integrity and Reliability. AMMRC MS 78-3, Army Materials & Mechanics Research Center, Watertown, Massachusetts, September 1978, pp. 63-82.
7. Smith, Howard W. "Fatigue Damage Indicator," United States patent No. 3,949,949, September 14, 1976.
8. Crane, R. L. et al. A Crack Growth Gage for Assessing Flaw Growth Potential in Structural Components. Wright-Patterson AFB, Ohio: Air Force Material Laboratory, October 1976. AFML-TR-76-174.
9. Torvik, Peter J. Applications of the Extremal Principles of Elasticity to the Determination of Stress Intensity Factors. Wright-Patterson AFB, Ohio: Air Force Institute of Technology, July 1977. AFIT TR77-3.
10. ----. "On the Determination of Stresses, Displacements and Stress Intensity Factors in Edge Cracked Sheets with Mixed Boundary Conditions," to appear in the Journal of Applied Mechanics.
11. Ori, J. A. Experimental Evaluation of a Single Edge Cracked Crack Growth Gage for Monitoring Aircraft Structure. MS Thesis. Wright-Patterson AFB, Ohio: Air Force Institute of Technology, December 1977.
12. Ashbaugh, N. E. and A. F. Grandt. Evaluation of a Crack Growth Gage for Monitoring Possible Structural Fatigue Growth. Wright-Patterson AFB, Ohio: Air Force Material Laboratory, May 1977. AFML-TR-77-233.

13. Evaluation of the Crack Gage Concept for Monitoring Aircraft Flaw Growth Potential. USAF/Boeing Wichita Contract No. F33615-77-C-5073.
14. Service Life Tracking Program - Crack Growth Gages. USAF/McDonnell Douglas Corp. Contract No. F42600-78-D-0014.
15. Williams, M. L. "Stress Singularities Resulting from Various Boundary Conditions in Angular Corners of Plates in Extension," Journal of Applied Mechanics, Trans. ASME, Vol. 74, December 1952, pp. 526-528.
16. ----- "On the Stress Distribution at the Base of a Stationary Crack," Journal of Applied Mechanics, Vol. 24, March 1957, pp. 109-114.
17. Fung, Y. C. Foundations of Solid Mechanics. New York: Prentice-Hall, Inc., 1965.
18. Bowie, O. L. et al. "Solution of Plane Problems of Elasticity Utilizing Partitioning Concepts." Trans. ASME, Series E., Journal of Applied Mechanics, Vol. 40, pp. 767-772, 1973.
19. Verkayya, V. B. and V. A. Tischler. ANALYZE - Analysis of Aerospace Structures with Membrane Elements, Wright-Patterson AFB, Ohio: Air Force Flight Dynamics Laboratory, August 1978. TM-F2R-78-89.
20. Rook and Cartwright. Stress Intensity Factors. London: Her Majesty's Stationary Office, 1976.
21. Tada, Hiroshi, P. C. Paris, and G. R. Irwin. The Stress Analysis of Cracks Handbook, Dell Research Corporation, Hellertown, PA, 1973.
22. Rice, J. R. "Stresses in an Infinite Strip Containing a Semi-Infinite Crack," Trans. ASME Series E., Journal of Applied Mechanics, Vol. 34, pp. 248-250, 1967.
23. Grandt, A. F. Dr. and Dr. N. E. Ashbaugh. Air Force Material Laboratories, Personal Communication, August - November 1978.

Appendix A

Stresses and Displacements as Result of Williams' Stress Function

For the symmetric type problems introduced, only the even part of Williams' stress function is of interest and may be expressed as:

$$\begin{aligned} \chi_e = & (-1)^{n-1} A_{2n-1} r^{n+1/2} \{-\cos(n-3/2)\theta + \frac{2n-3}{2n+1} \cos(n+1/2)\theta\} + \\ & + (-1)^n A_{2n} r^{n+1} \{-\cos(n-1)\theta + \cos(n+1)\theta\} \end{aligned} \quad (46)$$

σ_{rr} , $\sigma_{\theta\theta}$, $\sigma_{r\theta}$ are found by:

$$\sigma_{rr} = \frac{1}{r^2} \frac{\partial^2 \chi_e}{\partial \theta^2} + \frac{1}{r} \frac{\partial \chi_e}{\partial r} \quad (47)$$

$$\sigma_{\theta\theta} = \frac{\partial^2 \chi_e}{\partial r^2} \quad (48)$$

$$\sigma_{r\theta} = -\frac{1}{r} \frac{\partial^2 \chi_e}{\partial r \partial \theta} + \frac{1}{r^2} \frac{\partial \chi_e}{\partial \theta} \quad (49)$$

$$\begin{aligned} \sigma_{r\theta(1)} = & (-1)^{n-1} r^{n-3/2} A_{2n-1} (n-3/2) \cdot (n-1/2) \cdot \\ & \cdot \{\sin(n+1/2)\theta - \sin(n-3/2)\theta\} \end{aligned} \quad (50)$$

$$\sigma_{r\theta(2)} = (-1)^n r^{n-1} A_{2n} (n) \{(n+1)\sin(n+1)\theta - (n-1)\sin(n-1)\theta\} \quad (51)$$

$$\sigma_{r\theta} = \sigma_{r\theta(1)} + \sigma_{r\theta(2)} \quad (52)$$

$$\begin{aligned}\sigma_{rr(1)} = & (-1)^{n-1} r^{n-3/2} A_{2n-1} \cdot \{[(n-3/2)^2 - (n+1/2)] \cdot \cos(n-3/2)\theta \\ & - (n-3/2)(n-1/2) \cos(n+1/2)\theta\}\end{aligned}\quad (53)$$

$$\begin{aligned}\sigma_{rr(2)} = & (-1)^n r^{n-1} A_{2n} \cdot \{[(n-1)^2 - (n+1)] \cos(n-1)\theta - \\ & - n(n+1) \cos(n+1)\theta\}\end{aligned}\quad (54)$$

$$\sigma_{rr} = \sigma_{rr(1)} + \sigma_{rr(2)} \quad (55)$$

$$\begin{aligned}\sigma_{\theta\theta(1)} = & (-1)^{n-1} r^{n-3/2} A_{2n-1} (n+1/2)(n-1/2) \cdot \left\{ \frac{n-3/2}{n+1/2} \cos(n+1/2)\theta - \right. \\ & \left. - \cos(n-3/2)\theta \right\}\end{aligned}\quad (56)$$

$$\sigma_{\theta\theta(2)} = (-1)^n r^{n-1} A_{2n} (n)(n+1) \{ \cos(n+1)\theta - \cos(n-1)\theta \} \quad (57)$$

$$\sigma_{\theta\theta} = \sigma_{\theta\theta(1)} + \sigma_{\theta\theta(2)} \quad (58)$$

Solving the equation

$$\nabla^2 \chi_e = \frac{\partial}{\partial r} \left(r \frac{\partial \psi_e}{\partial \theta} \right) \quad (59)$$

get as a result

$$\begin{aligned}\psi_e = & (-1)^{n-1} \frac{r^{n-3/2}}{n-1/2} A_{2n-1} \cdot \left[\frac{(n-3/2)^2 - (n+1/2)^2}{n-3/2} \sin(n-3/2)\theta \right] + \\ & + (-1)^n \frac{r^{n-1}}{n} A_{2n} \cdot \left[\frac{(n-1)^2 - (n+1)^2}{n-1} \sin(n-1)\theta \right]\end{aligned}\quad (60)$$

Substitute in

$$2\mu U_r = \frac{\partial \chi_e}{\partial r} + (1-s)r \frac{\partial \psi}{\partial \theta} \quad (61)$$

$$2\mu U_\theta = -\frac{1}{r} \frac{\partial \chi}{\partial \theta} + (1-s)r^2 \frac{\partial \psi}{\partial r} \quad (62)$$

ν = Poisson ratio $s = \nu/(1 + \nu)$,

μ = shear modules.

As a result:

$$2\mu U_{r(1)} = (-1)^{n-1} r^{n-1/2} A_{2n-1} \left\{ \left[(n+1/2) + \frac{1-s}{(n-1/2)} \cdot [(n-3/2)^2 - (n-1/2)^2] \right] \cdot \right. \\ \left. \cdot \cos(n-3/2)\theta - (n-3/2)\theta \cos(n+1/2)\theta \right\} \quad (63)$$

$$2\mu U_{r(2)} = (-1)^n r^n A_{2n} \left\{ \left[(n+1) + \left(\frac{1-s}{n} \right) \cdot [(n-1)^2 - (n+1)^2] \right] \cdot \right. \\ \left. \cdot \cos(n-1)\theta - (n+1)\cos(n+1)\theta \right\} \quad (64)$$

$$2\mu U_r = 2\mu (U_{r(1)} + U_{r(2)}) \quad (65)$$

$$2\mu U_{\theta(1)} = (-1)^{n-1} r^{n-1/2} A_{2n-1} \left\{ \left[-(n-3/2) + \frac{1-s}{n-1/2} \cdot \right. \right. \\ \left. \left. \cdot [(n-3/2)^2 - (n+1/2)^2] \right] \sin(n-3/2)\theta + (n-3/2)\sin(n+1/2)\theta \right\} \quad (66)$$

$$2\mu U_{\theta(2)} = (-1)^n r^n A_{2n} \left\{ \left[-(n-1) + \frac{1-s}{n} \cdot [(n-1)^2 - (n+1)^2] \right] \cdot \right. \\ \left. \cdot \sin(n-1)\theta + (n+1)\sin(n+1)\theta \right\} \quad (67)$$

$$2\mu U_\theta = 2\mu (U_{\theta(1)} + U_{\theta(2)}) \quad (68)$$

Appendix B

Description of Computer Program

Three computer programs used to generate the stress intensity factor in this study will be described here. Program COEFDT was used to solve the trapezoid case. COEFINA was used to provide the solution for the center segment of the stepped gage. Program TAYLOR was used to match the segments of the stepped gage. A few subroutines are common to both COEFDT and COEFINA. The subroutines and parts of COEFDT and COEFINA were developed by Torvik for a previous analysis (Ref 9, 10).

Subroutine DPSI

In this subroutine tangential displacements in Eqs (66), (67) are evaluated. The results are transferred to the main program as for Eq (66) and Eq (67) separately.

Subroutine DR

In this subroutine radial displacements as in Eqs (63), (64) are evaluated.

Subroutine SPR

This subroutine evaluates radial stresses as in Eq (53), (54).

Subroutine STT

This subroutine evaluates tangential stresses as in Eqs (56), (57).

Subroutine SRT

This subroutine evaluates shear stress as in Eqs (50), (51).

Program COEFDT

This program evaluates the matrix A_{mq} as in Eq (24). The eval-

uation is done for each of the three edges of the three separately, and the results added to produce the required matrix element. The evaluation is made first on the uncracked edge, and last on cracked edge. Then F_q is evaluated on edge 2 via Eq (25). Finally, the system of Eq (23) is solved for d_m , and d_1 is the desired result.

Program COLFINA

This program evaluates the matrix A_{mq} via Eq (29) in the same order as done in program COEFDI. The vector F_q is evaluated on edge 2 via Eq (30) by moving a unit load from one nodal point to the other. F_q is evaluated n times as the number of nodal points. Solution of Eq (23) each time gives finally an array $\{D\}$ of coefficients d_{m1}^k . In parallel to the above described procedure, the program constructs the flexibility matrix $[Sc]$ for the center segment.

Program TAYLOR

This program evaluates K_I via Eq (40).

Appendix C

Finite Element Solution

The flexibility matrix for the outer segment of the gage was obtained by using a slightly modified version of the finite element analysis program "ANALYZE" (Ref 18). The problem was solved with a mesh that consisted of 452 nodes and 441 elements. The elements used were quadrilateral and triangular membranes. Mesh organization and boundary conditions are shown in Figure 23. As a check of the solution, displacements of the "pulled" edge were examined. The displacements at the edges looked extremely high in comparison with displacements at the center, but were found to agree with a second solution obtained through NASTRAN. Since in our case we have a very short membrane, width = 4, $L = 1.9; 1.27; 1.6; 2.0; 4.0$; and $t_0 = .08$, it was suspected that the restraint in the x direction has an effect of singularity. To check this point, the restraints in the x direction at nodes 1, 441 were released and then all restraints in x direction, except at the mid-node 221, were released. This modification did not change the results significantly, as can be seen in Figure 24. This suggests that no singularity effects were introduced by the x direction restraint. Figure 24 also shows the displacement variation as the length of the membrane grows.

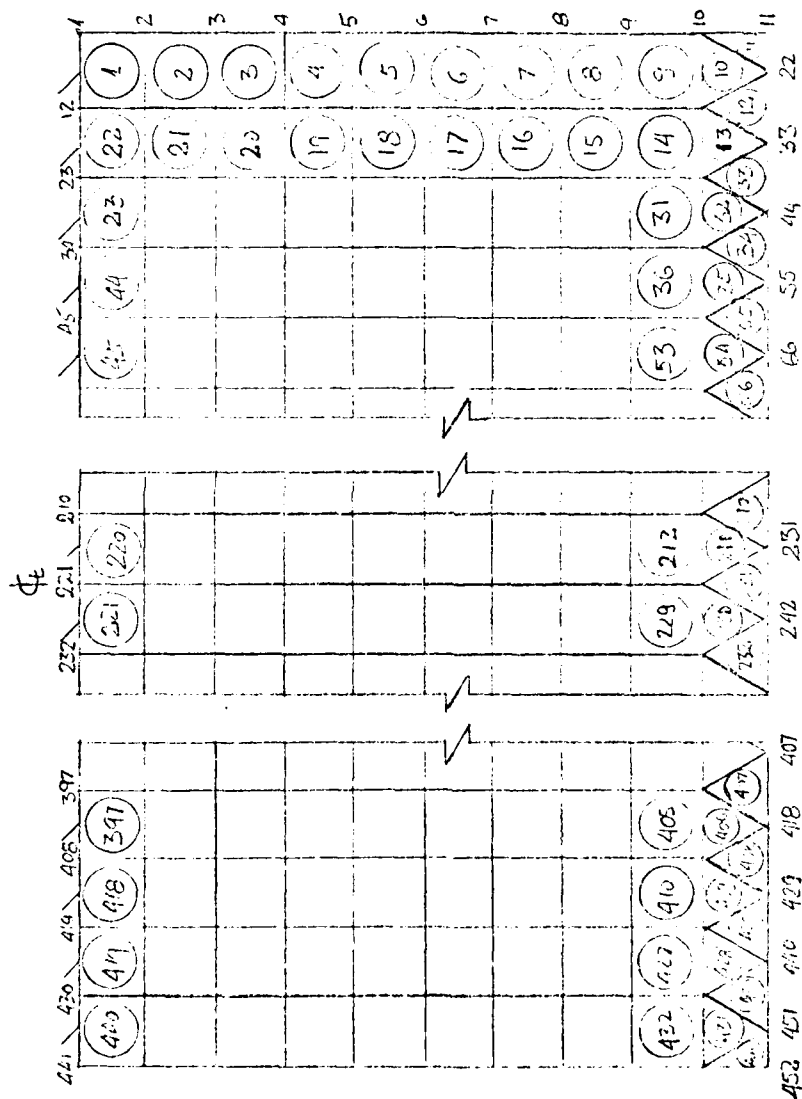


Figure 23. Finite Element Model and Mesh Organization for Outer Segment of Gage

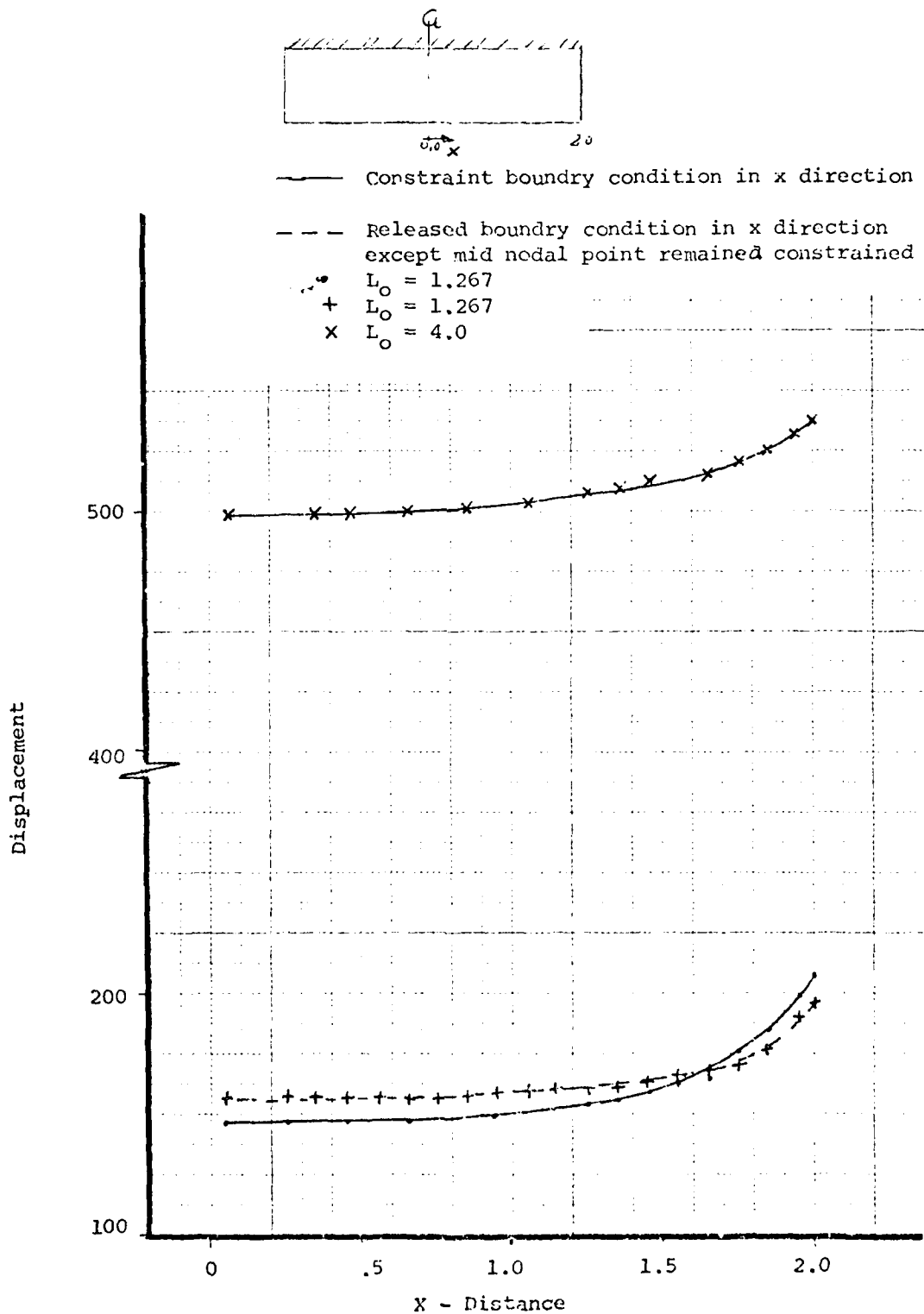


Figure 24. Displacements of Membrane Edge Due to Uniform Stress

Appendix D

Stepped Center Gage - Stress Intensity Factor Approximate Equation

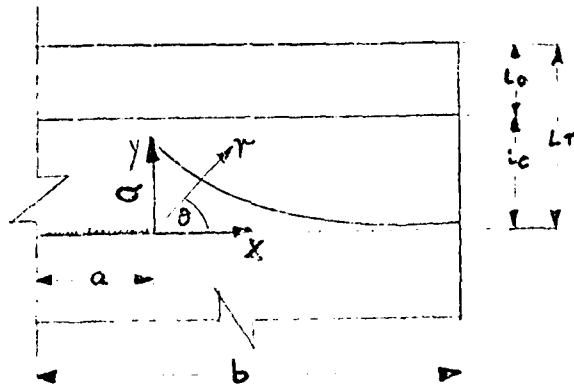


Figure 25. Schematic Stress Distribution at Crack Tip
of Stepped Gage

Using the relationship between stress intensity factor and stress,
on the line $y = 0$, we get:

$$\sigma = \frac{K_I}{\sqrt{2\pi x}} \quad (69)$$

and the force P_a produced over the uncracked region will be

$$P_a = \int_0^{b-a} \frac{2K_I}{\sqrt{2\pi x}} t_c dx \quad (70)$$

$$P_a = \sqrt{\frac{8}{\pi}} t_c \sqrt{b-a} K_I \quad (71)$$

This force will produce an average displacement on the outer segment of

$$U_o = \frac{P L_o}{A_o E_o} = \frac{P L_o}{b \cdot t_o E_o} \quad (72)$$

The displacement of the center segment, may be approximated by using Rice's (Ref 22:249) result for an infinite strip with semi-infinite crack,

$$U_c = \frac{K_I [(1 - \nu^2) L_c]^{1/2}}{E} \quad (73)$$

The total displacement may be expressed as

$$U_{tot} = U_c + U_o \quad (74)$$

On the other hand, U_{tot} produced by the displacement of the bond line with the carrying structure is

$$U_{tot} = \frac{L_t \sigma_s}{E} \quad (75)$$

Substituting and rearranging and making a nondimensional stress intensity factor, normalized with respect to the nominal stress in the structure we get:

$$\frac{K_I}{\sigma_s \sqrt{b}} = \frac{L_o + L_c}{\sqrt{b} \left[\frac{\sqrt{8}}{\pi} \frac{L_o}{b} \frac{t_c}{t_o} \sqrt{b-a} + \sqrt{(1-\nu^2) L_c} \right]} \quad (76)$$

Vita

Menachem Carmon was born on 27 October 1945, in Piatra Niamz, Romania. In 1950, he immigrated with his parents to Israel. He was graduated from Gymnasia Dvir High School in Ramat-Gan, Israel, in 1963. He entered the Technion, Israeli Institute of Technology through the ROTC program and was awarded a bachelor of science degree in Aeronautical Engineering in August 1967. He went through various assignments in the Israeli Air Force till he was selected to join the graduate program at AFIT on June 1977. He is married to the former Ella Barkan and they have a daughter Einat and a son Shay.

Permanent address: 61 Rambam Street
Raanana, Israel

UNCLASSIFIED

SECURITY CLASSIFICATION OF THIS PAGE (When Data Entered)

REPORT DOCUMENTATION PAGE		READ INSTRUCTIONS BEFORE COMPLETING FORM
1. REPORT NUMBER AFIT/GAE/AA/78D-3	2. GOVT ACCESSION NO.	3. RECIPIENT'S CATALOG NUMBER
4. TITLE (and subtitle) EFFECTS OF GEOMETRIC VARIABLES ON STRESS INTENSITY FACTORS FOR CRACK GAGES		5. TYPE OF REPORT & PERIOD COVERED MS Thesis
7. AUTHOR(s) Menachem Carnon Major, IAF		6. PERFORMING ORG. REPORT NUMBER
3. PERFORMING ORGANIZATION NAME AND ADDRESS Air Force Institute of Technology (AFIT/EN) Wright-Patterson AFB, Ohio 45433		8. CONTRACT OR GRANT NUMBER(s)
11. CONTROLLING OFFICE NAME AND ADDRESS Air Force Flight Dynamic Laboratories Wright-Patterson AFB, Ohio 45433		10. PROGRAM ELEMENT, PROJECT, TASK AREA & WORK UNIT NUMBERS
14. MONITORING AGENCY NAME & ADDRESS (if different from Controlling Office)		12. REPORT DATE December 1978
		13. NUMBER OF PAGES 74
		15. SECURITY CLASS. (of this report) Unclassified
		15a. DECLASSIFICATION/DOWNGRADING SCHEDULE
16. DISTRIBUTION STATEMENT (of this Report) Approved for public release; distribution unlimited		
17. DISTRIBUTION STATEMENT (of the abstract entered in Block 20, if different from Report)		
18. SUPPLEMENTARY NOTES Approved for public release, IAW AFR 190-17 JOSEPH P. HIRPS, Major, USAF Director of Information		
19. KEY WORDS (Continue on reverse side if necessary and identify by block number) crack gage stress intensity factor fatigue		
20. ABSTRACT (Continue on reverse side if necessary and identify by block number) A cracked metallic coupon, called crack gage, is being considered as a device for monitoring crack growth in aircraft structures. For this purpose, a stress intensity factor solution for the gage has to be known. This study provides stress intensity factor solutions for two basic geometric configurations subjected to prescribed displacements. 1. Edge cracked, trapezoidal shaped gages of uniform thickness. 2. Center cracked gages with varying or stepped thickness.		

UNCLASSIFIED

SECURITY CLASSIFICATION OF THIS PAGE (When Data Entered)

20. For the trapezoid, the influences of changing the length of the cracked edge, while other edge remains constant, and vice-versa, were investigated. The results obtained do not show significant beneficial changes in stress intensity factor for the range of parameters considered over those of rectangular gages.

Stress intensity factors were determined for stepped gages of various geometries. Various thickness ratios, length ratios and aspect ratios were considered, including the specific geometries of two gages now under development. In each case, the stress intensity factor was determined as a function of crack length.

Stress intensity factors were found to increase as the cracked center portion was made thinner, and as the length of the outer section was increased. The stepped gage was found to have the potential for tailoring the stress intensity factor. Finally, the analytical results of stress intensity factor were found to show good agreement with experimental results.

UNCLASSIFIED

SECURITY CLASSIFICATION OF THIS PAGE (When Data Entered)